Computational and experimental studies of reactive intermediates in glycosylation reactions

Remmerswaal, W.A.

Chapter 6

Competing C-4 and C-5-Acyl Stabilization of Uronic Acid Glycosyl Cations

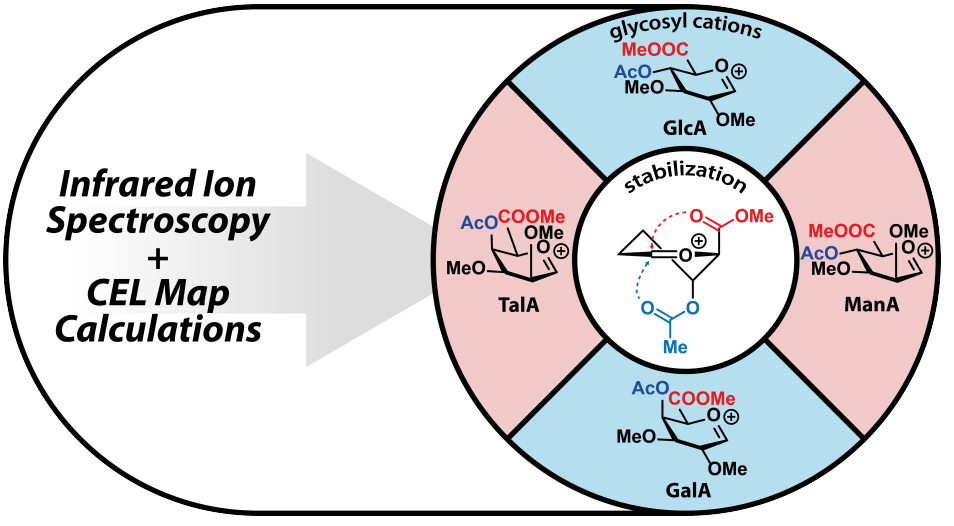

Abstract | Uronic acids, carbohydrates carrying a terminal carboxylic acid, have a unique reactivity in stereoselective glycosylation reactions. Herein, the competing intramolecular stabilization of uronic acid cations by the C-5 carboxylic acid or the C-4 acetyl group was studied with infrared ion spectroscopy (IRIS). IRIS reveals that a mixture of bridged ions is formed, in which the mixture is driven towards the C-1,C-5-dioxolanium ion when the C-5,C-2-relationship is *cis*, and towards the formation of the C-1,C-4-dioxepanium ion when this relation is *trans*. Isomer-population analysis and interconversion barrier computations show that the two bridged structures are not in dynamic equilibrium and that their ratio parallels the density functional theory-computed stability of the structures. These studies reveal how the intrinsic interplay of the different functional groups influences the formation of the different regioisomeric products.

Published | Elferink, H. *; Remmerswaal, W. A. *; Houthuijs, K. J. *; Jansen, O.; Hansen, T.; Rijs, A. M.; Berden, G.; Martens, J.; Oomens, J.; Codée, J. D. C.; Boltje, T. J. *Chem. Eur. J.* **2022**, 28, e202201724.

Introduction

The study of reactive intermediates formed in a chemical glycosylation is of major interest in carbohydrate chemistry to obtain insight into the stereoselective formation of glycosidic bonds. These intermediates are often highly reactive and may be extremely short-lived, making their characterization challenging. Using low-temperature NMR spectroscopy, Crich and co-workers were the first to identify and characterize anomeric triflates to support their intermediacy during glycosylation reactions.[1] Ever since, a wide variety of glycosyl triflates and related species have been reported.[2] The well-known directing effect of C-2-*O*-acyl groups has been substantiated by the identification of C-1,C-2-dioxolanium ions by trapping this bridged cation,[3] by observing the intermediate by NMR spectroscopy under reaction conditions[4] and by DFT computations.[5] Advances in NMR hardware and software have paved the way to characterize intermediates that are even less stable and present in only minute quantities in the reaction mixture, such as anomeric β-triflates,[6] dioxanium ions formed from non-vicinal acyl groups,[7] and reactive imidinium ions.[8,9] Despite these efforts, some intermediates are too unstable to be detected in solution, while there is strong indirect evidence for their role in the reaction mechanism.[10,11] For example, oxocarbenium ions[12,13] and glycosyl cations stabilized by non-vicinal acyl groups have often been invoked as product-forming intermediates.[14] Oxocarbenium ion intermediates have been studied extensively with computational chemistry,[5] superacid chemistry,[15,16] infrared ion spectroscopy (IRIS)[17,18] and combinations thereof.[19] While the existence of glycosyl cations stabilized by non-vicinal esters is a heavily debated topic,[14,20,21] their formation and structure in the gas-phase has recently been well established through IRIS[22–25] and computational studies.[5,26–31] Using a combination of IRIS, DFT calculations and a systematic series of model glycosylations, the potential role of non-vicinal esters in glycosylation reactions was assessed to find that the formation and stability of ester-stabilized ions was highly dependent on the configuration of donor glycosides and the position on which the participating acyl group was mounted. It was found that, in case of C-3-acyl-mannosyl donors, the formation of a bridged dioxanium ion was most pronounced and it was subsequently shown to exist under relevant glycosylation conditions using chemical exchange saturation transfer NMR.[7]

Another example of anchimeric assistance of non-vicinal esters can be found in uronic acids, monosaccharides that carry a C-5 carboxyl group. Uronic acids are an important class of carbohydrates that are key components in various biomolecules, including the glycan chains of saponins, glycosaminoglycans, bacterial polysaccharides, pectins and alginates.[32] Therefore, they have been attractive targets for synthesis. It has been shown that C-5-carboxylate esters, present in uronic acid donors, can intercept oxocarbenium ions to form C-1,C-5-dioxolanium ions.[17,18] In a previous study on the formation of oxocarbenium and dioxolanium ions from a 4-*O*-acetyl mannuronic acid donor, formation of a major C-1,C-5-dioxolanium ion species, alongside a minor C-1,C-4-dioxepanium ion species, was observed.[29] Both bridged ions can readily form from the $^{3}H_{4}$ oxocarbenium, which represents the most stable mannuronic acid oxocarbenium ion conformer, placing the C-3, C-4 and C-5 groups in *pseudo*-axial positions, allowing them to donate electron density towards the anomeric center.[33–35] To understand the stereoelectronic factors that determine the relative stability of the regioisomeric ions formed from C-4-acetyl uronic acid donors, this chapter reports a study on a set of glycosyl cations, generated from uronic acid donors, differing in stereochemistry at the C-2 and C-4 position. The focus was placed on the most common type of pyranosyl uronic acids, *i.e.,* glucuronic acid (GlcA), galacturonic acid (GalA) and mannuronic acid (ManA), but taluronic acid (TalA) was also included, considering that it shares the axial orientation of the C-4 group with GalA and the orientation of the axial C-2 hydroxy group with ManA.[36] The ions generated from these donors were studied by combining IRIS with quantum-chemical computations.

The glycosyl cations were generated by tandem-MS and characterized by IRIS. The IR-ion spectra have revealed that both the C-1,C-4- and C-1,C-5-bridged ions can be formed, and that the preferred isomer critically depends on the configuration at C-2. GlcA and GalA donor led to the preferential formation of C-1,C-4-dioxepanium ions, while ManA and TalA donors mainly provided C-1,C-5-dioxolanium ions. The mixture of bridged ions could be disentangled by a population analysis to establish their relative ratio. Furthermore, the ratio of the bridged ions could be correlated to the relative stability of the ions, as revealed by conformational energy landscape (CEL) maps created using DFT computations. These results demonstrate the impact of the relative stereochemistry on the preferred stabilization by acyl groups on uronic acid donors and may lead to the development of new stereoselective glycosyl donors.

Results and Discussion

The set of donor glycosides, **1—4**, used in this study is depicted in Figure 1 (see SI for a detailed description of the synthesis of new compounds).[37] Because the generation of the GalA and TalA glycosyl cations from the parent thioglycosides by collision induced dissociation (CID) produced a complex fragmentation pattern, the corresponding sulfoxide donors were generated for these two pyranosides. These donors ionize more readily and prevent alternative fragmentation pathways that lead to loss of overall signal. Previously, the participation of non-vicinal esters in the glucose, galactose and mannose series was investigated, and it was reported that both the C-4-acetyl glucosyl and galactosyl donors provide C-1,C-4-dioxepanium ions upon ionization and CID. By contrast, ionization and CID on the C-4-acetyl mannose donor led to the formation of a ring-opened C-4,C-5-dioxolanium ion.[29] The ions formed from the analogous C-4-acetyl talose donor **5** have not been reported yet. To relate the structure of the ions generated from the C-4-acetyl TalA donor **4** to the structure of the ions lacking the C-5 carboxylic acid ester, donor **5** was generated and the glycosyl cations derived from this precursor were studied.

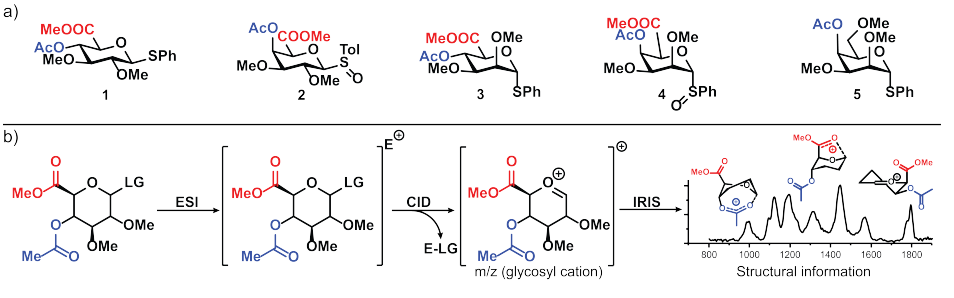

Figure 1. a) Ion precursors (**1**–**5**) used for IRIS-experiments. b) General overview of the workflow to generate and characterize glycosyl cations by IR-ion spectroscopy (IRIS). PG=protecting group, LG=leaving group, and E=ammonium or proton.

IR ion spectroscopy of uronic acid cations

The cations generated from **1—5** were characterized with IR ion spectroscopy using the FELIX infrared free electron laser operating between 750 and 1900 cm^{-1}.[38] This frequency range is well suited to distinguish between potential cation isomers: the glycosyl oxocarbenium ion, the C-1,C-4-dioxepanium ion and the C-1,C-5-dioxolanium ion. A significant difference in the O-C^+-O stretch is found between the C-1,C-4-dioxepanium ion (~1550 cm^{-1}) and the C-1,C-5-dioxolanium ion (~1650 cm^{-1}), which results from the difference in the vibration of the endocyclic vs. exocyclic OR group. Density-functional theory (DFT) and wave-function theory (WFT) computations were used to aid in the spectral assignment. Geometries and vibrational spectra of the cations were computed at the MP2/6-311++G(2d,2p)//B3LYP/6-31++G(d,p) level, which was found to model the vibrational frequencies well.[17,18,39] IR-ion spectra (Figure S1 and S2) were recorded of GlcA cation **6**, GalA cation **7**, ManA, cation **8,** talose cation **9** (for reference purposes, see the section on IR-ion spectroscopy in the supporting information**)** and TalA cation **10**, and assigned (Table S1). In the IR-ion spectra of the GlcA cation **6** and GalA cation **7** a high intensity band at 1550 cm^{-1} was observed, corresponding to the O-C^+-O stretch of an endocyclic C-1,C-4-dioxepanium ion. Of note, minor bands of the C-1,C-5-dioxolanium ion (most notably at 1650 cm^{-1}) were observed in the spectra of the GlcA and GalA ions **6** and **7**. In contrast, in the IR-ion spectra of the ManA and TalA cations **8** and **10,** a high intensity band at 1650 cm^{-1} was observed, corresponding to the C-1,C-5-dioxolanium ion. In turn, minor bands of the C-1,C-4-dioxepanium ion (most notably at 1550 cm^{-1}) were observed in the spectra of the Man and TalA ions.

To estimate the contribution of the minor species, the weighted average was optimized by minimizing the root-mean-square deviation between the experimental spectrum and the averaged computed spectra.[40] This methodology for estimating the contribution of the minor species was validated by comparison to experimentally determined isomer population analysis (Figure S3). Of note, during this isomer population analysis, it was possible to deplete the mixture of either component selectively, which indicates that under the experimental conditions the C-1,C-4- and C-1,C-5-bridged ions do not equilibrate on the experimental time-scale of 2 seconds (20 laser pulses at 10 Hz). For GlcA and GalA ions **6** and **7,** the contribution of the C-1,C-5-dioxolanium ion to the total population was, respectively, 9 % and 20 %, while for ManA and TalA ions **8** and **10,** the contribution of the C-1,C-5-dioxolanium ion to the total population was respectively 77 % and 66 % (Table 1). Thus, the GlcA and GalA ions **6** and **7** predominantly formed C-1,C-4-dioxepanium ions, while the ManA and TalA ions **8** and **10** favored formation of the C-1,C-5-dioxolanium ion.

Table 1. Summary of IR-ion spectroscopy results

Glycosyl Cation	Dominant carbonyl R-C-O-(C1) stretch	% C-1,C-4 dioxepanium	% C-1,C-5 dioxolanium
6 (Glucuronic acid)	~1550 cm^{-1} (4-O-C-O)	91 %	9 %
7 (Galacturonic acid)	~1550 cm^{-1} (4-O-C-O)	80 %	20 %
8 (Mannuronic acid)	~1650 cm^{-1} (6-C-OMe)	23 %	77 %
10 (Taluronic acid)	~1650 cm^{-1} (6-C-Ome)	34 %	66 %

CEL maps of glycosyl cations

To understand the preference for the formation of C-1,C-4 or C-1,C-5 bridged ions, the stability of these ions was computationally investigated. Recently, the relative stability of glycosyl cations was assessed, in which ester participation and oxocarbenium ion formation were in competition, using a DFT protocol to compute the conformational energy landscape (CEL) for these ions.[19,41] This method maps the energy of glycosyl cations as a function of their shape by probing the complete conformational space that these cations can occupy, see Figure 2a.[42,43] Here, four key rotamers were taken into account, differing in (1) the orientation of the C-4 acetate group, pointing either towards the anomeric C-1 (rotamer 1; R1) or away from C-1 (rotamer 2, R2), and (2) the orientation of the C-5 uronic acid moiety, pointing either towards C-1 in an eclipsed conformation (ecl) or away from C-1 in a bisected conformation (bis). Thus four rotamers were assessed, *i.e.*, R1-ecl, R1-bis, R2-ecl, and R2-bis (Figure 2b). The CEL maps were computed in the gas-phase using MP2/6-311++G(2d,2p)//B3LYP/6-311G(d,p), as this method was shown to provide accurate energies which correlate well with experimental results[19] (for more information see the Supporting Information). Figure 2 depicts the CEL maps of the four uronic acids: GlcA (Figure 2c), GalA (Figure 2d), ManA (Figure 2e) and TalA (Figure 2f), in which the R1-ecl is shown on the left side and R2-ecl rotamers on the right side. The bisected C-5 carboxylate rotamers for the glycosyl cations were computed to be significantly higher in energy for all isomers and are therefore not depicted (see Supporting Figure S6 and S7 for all CEL maps).

The CEL maps show that GlcA and GalA have a strong preference for the formation of a C-1,C-4-dioxepanium ion ($\Delta\Delta G°$=2.1 and 4.8 kcal mol^{-1}, respectively) over other cations, with the GlcA C-1,C-4-dioxepanium ion preferentially taking up a $^{5}S_{1}$-like conformation and the GalA C-1,C-4-dioxepanium ion in a $^{1}S_{5}$-like skew boat form. In contrast, for ManA and TalA, the CEL maps show that the C-1,C-5-dioxolanium ions in a $^{1}C_{4}$-like conformation are more favorable ($\Delta\Delta G°$=3.2 and 0.3 kcal mol^{-1}). The maps reveal that the TalA C-1,C-4 and C-1,C-5 bridged ions are very close in energy. From the lowest energy structures, it can be deduced that the orientation of the C-2-substituent plays an important role in shaping the stability of the C-1,C-5-dioxiolanium ions. In the ManA and TalA ions, the C-2-OMe group takes up a sterically favorable *pseudo*-equatorial position. Hyperconjugative stabilization by donation of electron density of the axial σ_{C2-H2} bond in the σ^*_{C1-O+} (a stabilizing gauche effect) may also contribute favorably.[44] The GlcA and GalA C-1,C-5-dioxolanium ions, on the other hand, place their C-2-substituents in an unfavorable axial position. In the TalA and ManA C-1,C-4-dioxepanium ions, the C-2- and C-3-groups experience destabilizing eclipsing interactions, which are absent in the GlcA and GalA C-1,C-4-dioxepanium ions. The lowest energy structures of the GlcA and ManA C-1,C-4- and C-1,C-5-dioxolanium ions can be found in the same region of the CEL map, because the relative orientation of the C-4 and C-5 substituents is *trans*. In contrast, the C-1,C-4- and C-1,C-5 bridged ions in the GalA and TalA case, having *cis* C-4 and C-5 groups, are found in opposite regions of the conformational space. Thus, greater conformational changes are required for the interconversions between the two conformations for GalA and TalA than for GlcA and ManA, likely requiring a higher interconversion barrier.

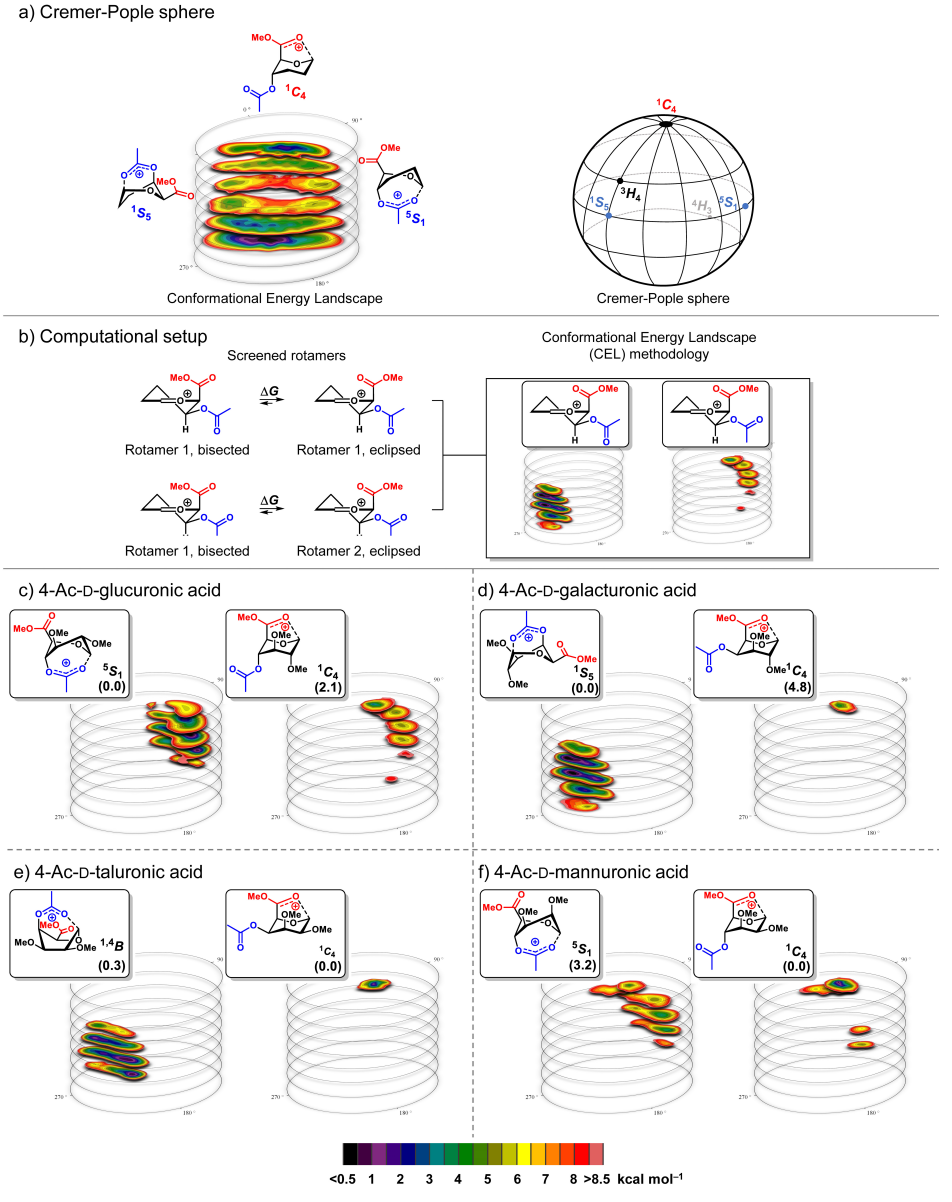

Figure 2. CEL maps of 2,3-*O*-Me-4-*O*-Ac-d-uronic acid cations in which the local minima identified are shown with their respective energy. a. The Cremer-Pople sphere. b. The used computational protocol. Two acetyl ester (R1 and R2) and two methoxy-acid rotamers (eclipsed and bisected) were considered for all computed glycosyl cations generating four CEL maps (R1 bisected, R1 eclipsed, R2 bisected, R2 eclipsed). Only eclipsing methoxy-acid rotamers are shown because they are lower in energy than the corresponding bisecting rotamers. All energies are as computed at MP2/6-311++G(2d,2p)//B3LYP/6-311G(d,p) at 298.15 K and expressed as gas-phase Gibbs free energy in kcal mol^{-1}. CEL maps for (c) glucuronic acid, (d) galacturonic acid, (e) taluronic acid, and (f) mannuronic acid cations.

Computing the interconversion between bridged glycosyl cation conformations

To explore the conformational change required for the interconversion between the C-1,C-4-dioxepanium and C-1,C-5-dioxolanium ions, the reaction profile of this interconversion (Figure 3) was computed (see Supporting Table S1 for the complete reaction profiles). The interconversion between these structures, starting from the C-1,C-4-dioxepanium ion, occurs through a series of conformational changes. These transformations are not necessarily limited to a certain order, so multiple possible routes were computed and evaluated. Scheme 1 contains an overview of the relevant intermediates for this interconversion (See Table S1 for all energies of the intermediates and transition states). For each cation, two global pathways were evaluated: direct interconversion between the C-1,C-4-dioxepanium and C-1,C-5-dioxolanium ions through an intramolecular S_N2-like reaction, and a more step-wise pathway proceeding through oxocarbenium ion intermediates. Various orders of the steps of the latter pathway are possible for both 4,6-*trans* (GlcA and ManA) and 4,6-*cis* (GalA and TalA) uronic acid cations, and these were all computed (Scheme 1). Figure 3 and 4 show the most favorable interconversion for GlcA, GalA, ManA and TalA cations **6**—**9** (occurring through the overall lowest path) between the C-1,C-4-dioxepanium (**1-INT**) and C-1,C-5-dioxolanium ions (**5-INT**).

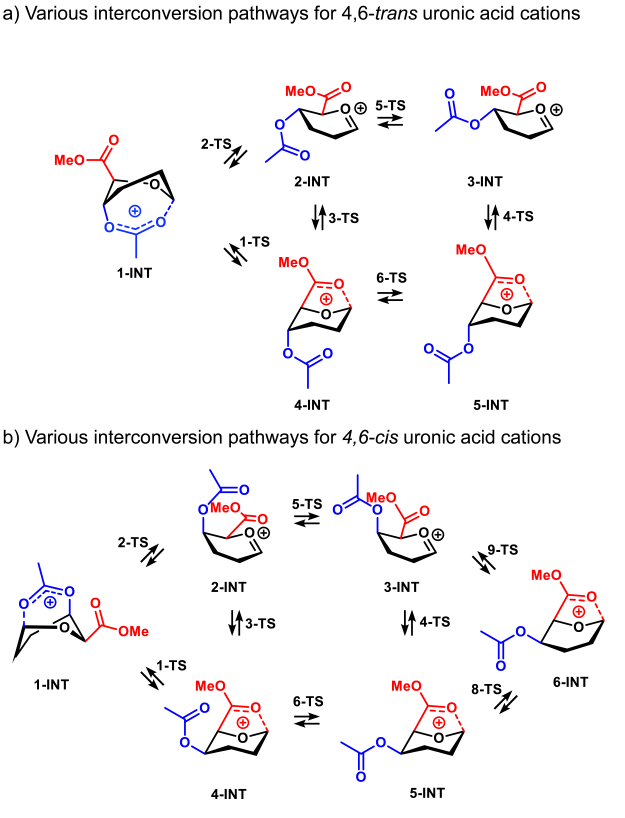

Scheme 1. a) The interconversion between the C-1,C-4-dioxepanium and C-1,C-5-dioxolanium ions pathways for 4,6-*trans* epimers (GlcA and ManA cations **6** and **8**). b) The interconversion between the C-1,C-4-dioxepanium and C-1,C-5-dioxolanium ions pathways for 4,6-*cis* epimers (GalA and TalA cations **7** and **10**).

First the interconversion of the 4,6-*trans* epimers GlcA and ManA cations **6** and **8** (Scheme 1a and Figure 3) were examined. Both cations interconvert through the 'direct substitution' pathway. Starting from the C-1,C-4-dioxepanium (**1-INT**), the uronic acid carbonyl moiety directly attacks the anomeric center (**1-TS**), transitioning to a $^1C_4$ conformation in the process, and forms C-1,C-5-dioxolanium ion intermediate **4-INT**. For both GlcA and ManA this step is the rate-limiting step, with barriers of +14.3 and +13.8 kcal mol^{-1}, respectively. The C-4-OAc ester group then rotates around the H4-C4-O4-C_{acetyl} bond (**5-TS**), transitioning the H4-C_{acetyl} relation from an *anti*-orientation towards the more stable *syn*-orientation, forming the C-1,C-5-dioxolanium ion (**5-INT**). For the GalA and TalA cations **7** and **10** (Scheme 1b and Figure 4), this direct substitution pathway is not viable because the acetyl group is positioned on the same side as the uronic acid, leading to exceedingly high barriers.[45] Instead, the O_{acetyl}-C1 bond first dissociates (**2-TS**), forming an oxocarbenium ion intermediate in which the H4-C_{acetyl} relation is *anti* (**2-INT**). For GalA, the uronic acid carbonyl group then associates with C-1 (**3-TS**), forming C-1,C-5-dioxolanium ion intermediate **4-INT**, followed by rotation of the C-4 acetate ester group around the H4-C4-O4-C_{acetyl} bond (6-**TS**), forming the C-1,C-5-dioxolanium ion (**5-INT**). The rate-determining step in this pathway, is the dissociation of the C-4 acetate ester (**2-TS**, +18.4 kcal mol^{-1}). For the TalA oxocarbenium ion (**2-INT**) the C-4 acetate ester group first rotates around the H4-C4-O4-C_{acetyl} bond (**5-TS**) transitioning the H4-C_{acetyl} relation to a *syn* orientation (**3-INT**). The uronic acid carbonyl then associates with C-1 (**9-TS**) to form the boat-shaped intermediate (**6-INT**), which then relaxes (**8-TS**) forming the C-1,C-5-dioxolanium ion (**5-INT**). Although the rate-determining step in this pathway is the rotation of the acetate group (**5-TS**, +23.5 kcal mol^{-1}), other pathways have similar barrier heights resulting from steric crowding of the TalA cation. The computed high barrier height for the interconversions of TalA and GalA are in line with the observations from isomer population analysis experiments, in which the C-1,C-4- and C-1,C-5-bridged ions do not equilibrate on the two second time-scale of that experiment.[46]

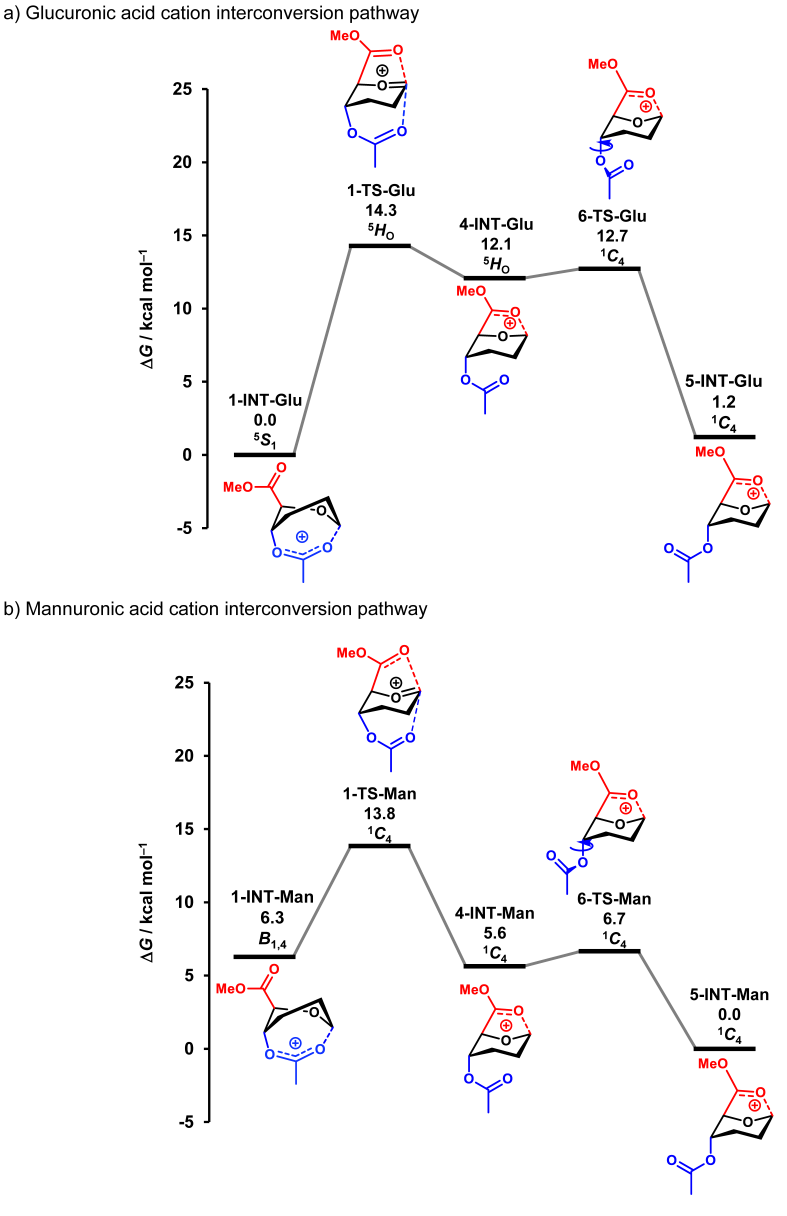

Figure 3. Reaction profile of the interconversion between the C-1,C-5-dioxolanium and C-1,C-4-dioxepanium ions for 2,3-OMe-4-OAc-D-glucuronic (a) and -mannuronic (b) acid. All energies are as computed at MP2/6-311++G(2d,2p)//B3LYP/6-311G(d,p) at 298.15 K and expressed as gas-phase Gibbs free in kcal mol^{-1}. For visual clarity, the C-2 and C-3 side groups are not drawn.

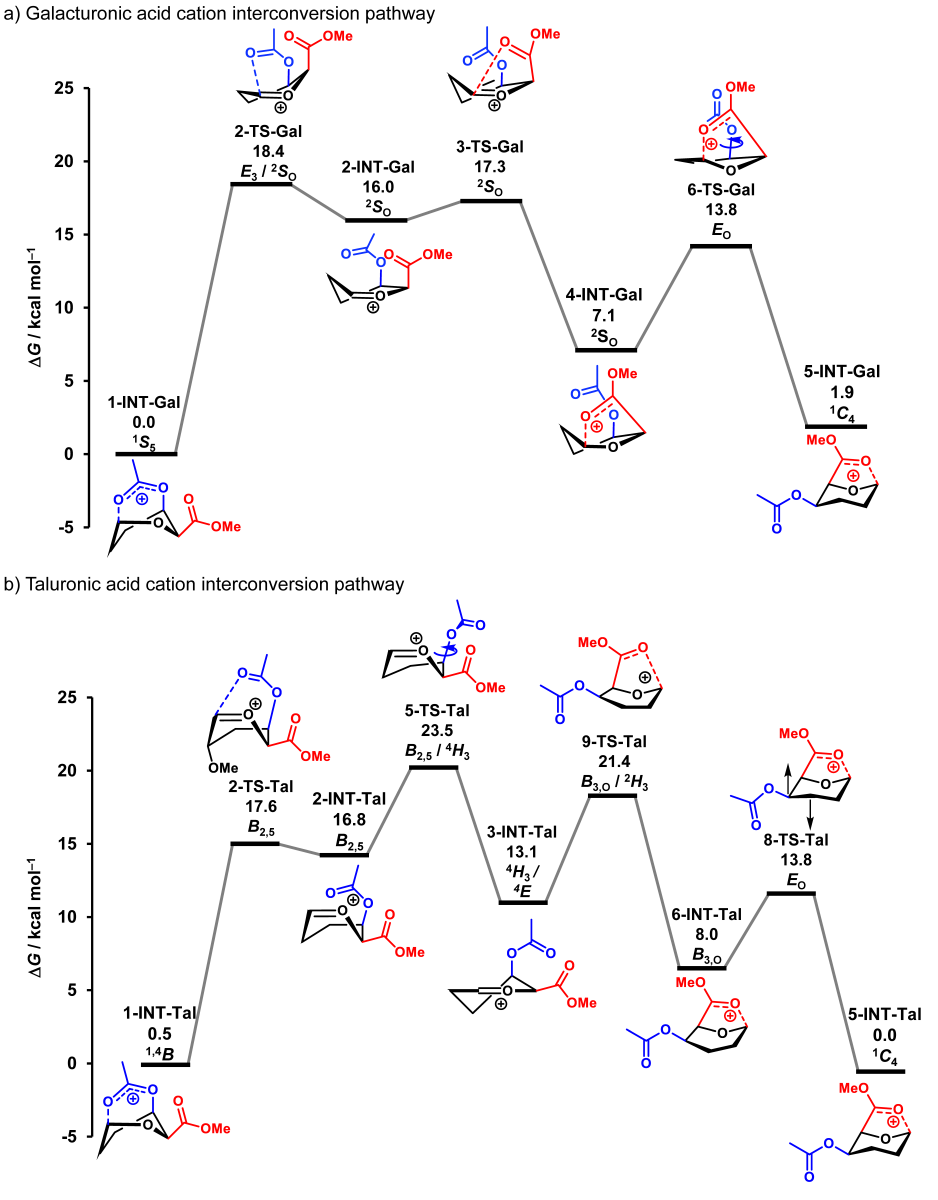

Figure 4. Reaction profile of the interconversion between the C-1,C-5-dioxolanium and C-1,C-4-dioxepanium ions for 2,3-OMe-4-OAc-D-galacturonic (a) and -taluronic (b) acid. All energies are as computed at MP2/6-311++G(2d,2p)//B3LYP/6-311G(d,p) at 298.15 K and expressed as gas-phase Gibbs free in kcal mol^{-1}. For visual clarity, the C-2 and C-3 side groups are not drawn.

Conclusions

Through a combination of IR ion spectroscopy and quantum-chemical computations, the formation of uronic acid cations carrying a C-4-acyl group was studied to unravel the stabilization of uronic acid oxocarbenium ions by either the C-5-carboxylate or C-4-ester. A relationship between the formation of either a C-1,C-5 or C-1,C-4-bridged ion and the relative configuration of C-2 and C-5 was discovered. The competitive formation of the C-1,C-5 or C-1,C-4 bridged ions is driven towards the C-1,C-5-dioxolanium ion when the C-5,C-2-relationship is *cis*, as present in the mannuronic and taluronic acid, and towards the formation of the C-1,C-4-dioxepanium ion when this relation is *trans*, as in glucuronic and galacturonic acid. The distribution of the formed dioxolenium ions depends on the stability of both isomeric ions, and they are not in equilibrium under the experimental conditions of the IRIS experiments as determined by the isomer population analysis and in line with DFT computations. The CEL maps revealed structural features that play a role in determining the stability of the different glycosyl cations, notably that the OMe at C-2 is consistently oriented equatorially to allow for hyperconjugative stabilization by donation of electron density of the axial σ_{C2-H2} bond in the σ^*_{C1-O+}. Insight into the structure of glycosyl cations is of relevance to understand the reactivity and stereoselectivity of glycosyl donors in the assembly of oligosaccharides and glycoconjugates. Even though the ions under study here were generated in the gas-phase, and the results of the study can therefore not be translated directly to a role in glycosylation reactions in solution, the study has revealed how the intrinsic interplay between different functional groups in these ions shapes their overall conformation and stability. The fact that C-1,C-4-, and C-1,C-5-bridged ions can be formed and observed might be exploited in glycosylation reactions in which the reactivity and stereoselectivity of uronic acid donor glycosides can be controlled by the installation of even more powerful participating acyl-type functionalities.[47–49]

Supporting information

Supporting Methods

Ion spectroscopy in a modified ion trap mass spectrometer

The experimental apparatus is based on a modified 3D quadrupole ion trap mass spectrometer (Bruker, AmaZon Speed ETD) that has been coupled to the beam line of the FELIX infrared free electron laser (IR-FEL).[38,50] Ammonium adducts of each compound ($[M+NH_4]^+$) were generated by electrospray ionization from solutions of 10^{-6} M (in 50:50 acetonitrile:water for compound **2** and 50:50 methanol:water for all other measured compounds) containing 2% ammonium acetate and introduced at 2 µl min^{-1}. The mass-isolated ions of interest were collisionally activated for 40 ms with an amplitude parameter of 0.2-0.4V in order to generate the relevant oxonium products. These fragment ions were subsequently mass isolated in an additional MS/MS stage and finally irradiated by the tunable mid-infrared beam. The FEL was tuned to provide 5 µs optical pulses at 10 Hz having 30–60 mJ pulse energy over the entire tuning range (bandwidth ~0.4% of the centre frequency). The pulse energy used for measurements was appropriately attenuated in order to avoid saturation of the signal. When a sufficient number of photons is absorbed, typically during a single macropulse, unimolecular dissociation occurs and generates frequency-dependent fragment ion intensities in the mass spectrometer. Relating the precursor ion intensity to the total fragmentation intensity in the observed mass spectra (according to Equation S1) for each frequency position generates an infrared vibrational spectrum (3 cm^{-1} step size). The yield is obtained from several averaged mass spectra and is linearly corrected for laser power; the IR frequency is calibrated using a grating spectrometer.

$$yield = \frac{-\ln(1 - \sum I\ (fragment\ ions))}{\sum I\ (parent + fragment\ ions)} \quad \text{(S1)}$$

Generation of computational IR spectra

Vibrational spectra of the candidate geometries were generated using a previously reported workflow.[29,51] A SMILES code for the oxocarbenium, C-1,C-4-dioxepanium, C-1,C-5-dioxolanium and ring-opened ions served as input for the cheminformatics toolbox RDKit.[52] For each ion, 500 random conformations were generated using the distance geometry algorithm, which were minimized using the MMFF94 classical forcefield. The 40 most distinct geometries were selected based on the root-mean-squared distance between them. The geometries

served as input for semi-empirical PM6 minimization and vibrational analysis with Gaussian16 Rev. C.01.[53] The resulting geometries were filtered for duplicates and subsequently minimized at the B3LYP/6-31++G(d,p) level, followed by vibrational analysis. More accurate enthalpies were obtained with single-point calculations at the MP2/6-311++G(2d,2p) level. The harmonic vibrational line spectra were frequency scaled by 0.975 and broadened using a Gaussian function with a full-width at half-maximum of 25 cm^{-1}, as to match the experimental peak widths.

Optimization of computational mixtures

The mixtures of the C-1,C-4-dioxepanium and C-1,C-5-dioxolanium computed spectra were optimized following the procedure of Barnes *et al.*[40] To generate the mixed spectra, the unnormalized stick spectra were frequency scaled and convoluted with a Gaussian function as above. As a starting point a 50:50 mixture of the computed spectra was used, and the resulting spectrum was then normalized. The mixing ratio was then optimized to give a minimal root-mean-squared-deviation between the mixed computed spectrum and experimental spectrum using the scikit-learn package.[54]

Generation of conformational energy landscapes (CEL).

The initial structure for the conformational energy landscape (CEL) mapping of the six-membered glycosyl cation was optimized by starting from a 'conformer distribution search' option included in the Spartan 14[55] program by utilizing MM as the level of theory and MMFF[56] as the method. All generated geometries were re-optimized with Gaussian 09 Rev. D.01[57] by using B3LYP/6-311G(d,p), after which a vibrational analysis was computed to obtain the thermodynamic properties. The geometry with the lowest energy was selected as the starting point for the CEL. A complete survey of the possible conformational space was done by scanning three dihedral angles ranging from −60° to 60°, including the C1-C2-C3-C4 (D1), C3-C4-C5-O (D3) and C5-O-C1-C2 (D5). The resolution of this survey is determined by the step size which was set to 15° per puckering parameter, giving a total of 729 prefixed conformations per glycosyl cation spanning the entire conformational landscape. All other internal coordinates were unconstrained. Except when a C2-substituent was present on the oxocarbenium ring of interest, then the C2-H2 bond length was fixed based on the optimized structure to counteract rearrangements occurring for higher energy conformers. The 729 structures were optimized in the gas-phase with B3LYP/6-311G(d,p), after which a vibrational analysis was computed to obtain the thermodynamic properties.[19,31,58] The final electronic energy was computed at MP2/6-311++G(2d,2p). For this specific study four rotamers were taken into account, depending on the orientation of the C-4 acetyl protecting group (R1, C=O oriented towards C-1, in a way that makes C-1,C-4-dioxepanium ion formation geometrically feasible. R2, C=O oriented away from C-1, in a way that makes C-1,C-4-dioxepanium ion formation geometrically impossible.) and the C-5 methoxy ester (Eclipsed, C=O oriented towards C-1 in a way that makes C-5,C-1 dioxolanium ion formation geometrically feasible. Bisected, C=O oriented away from C-1, in a way that makes C-5,C-1 dioxolanium ion formation geometrically impossible.). Giving four rotamers: R1-bisected (C-1,C-4-dioxepanium ion with C-5 C=O oriented away from C-1), R1-eclipsed (C-1,C-4-dioxepanium ion with C-5 C=O oriented towards C-1), R2-bisected (Oxocarbenium ion, both C=O groups orientated away from C-1), R2-eclipsed (C-1,C-5 dioxolaniun ion with C-4 C=O oriented away from C-1). For each rotamer CEL maps were separately computed and visualized. The $\Delta G^{T}_{gas,QH}$ were computed using the quasi-harmonic approximation in the gas-phase according to the work of Truhlar.[59] The quasi-harmonic approximation is the same as the harmonic oscillator approximation except that vibrational frequencies lower than 100 cm^{-1} were raised to 100 cm^{-1} as a way to correct for the breakdown of the harmonic oscillator model for the free energies of low-frequency vibrational modes. All optimized structures were checked for the absence of imaginary frequencies. To visualize the energy levels of the conformers on the Cremer-Pople sphere, slices were generated dissecting the sphere that combine closely associated conformers. The OriginPro software was employed to produce the energy heat maps, contoured at 0.5 kcal mol^{-1}.[60] For ease of visualization, the Cremer-Pople globe is turned 180° with respect to its common representation.

Supporting IR experiments and figures

IR ion spectroscopy of uronic acid cations

The measured IR-ion spectra of the GlcA cation **6** and GalA cation **7** are shown in Figure S1a-d (black line) and they contain several diagnostic peaks. In contrast to the IR ion spectrum of the ManA cation **8** (depicted in Figure S1e—f), a high intensity band at 1550 cm^{-1} is observed, corresponding to the O-C^{+}-O stretch of an endocyclic C-1,C-4-dioxepanium ion. Comparison with the calculated spectra of the C-1,C-4-dioxepanium (filled blue spectra) and C-1,C-5-dioxolanium (filled red spectra) ion shows good overlap for the former ion. Of note, minor bands (most notably at 1650 cm^{-1}) are observed in the spectra of the GluA and GalA ions, which suggest a mixture of species in which the C-1,C-5-dioxolanium ion is present as a minor fraction. Indeed, an improved spectral match is obtained from a weighted average of the computational spectra of the C-1,C-4-dioxepanium and C-1,C-5-dioxolanium ions (see Supporting Figure S4). The optimum mixing ratio is determined by minimizing the root-mean-square deviation between the experimental spectrum and the averaged computed spectra,[40] giving 9 % and 20 % contributions of the C-1,C-5-dioxolanium ion to the total population for GluA and GalA, respectively. In both cases, the calculated spectra of the oxocarbenium and previously observed ring-opened ions show poor overlap with the measured spectra (see Supporting Figure S5).

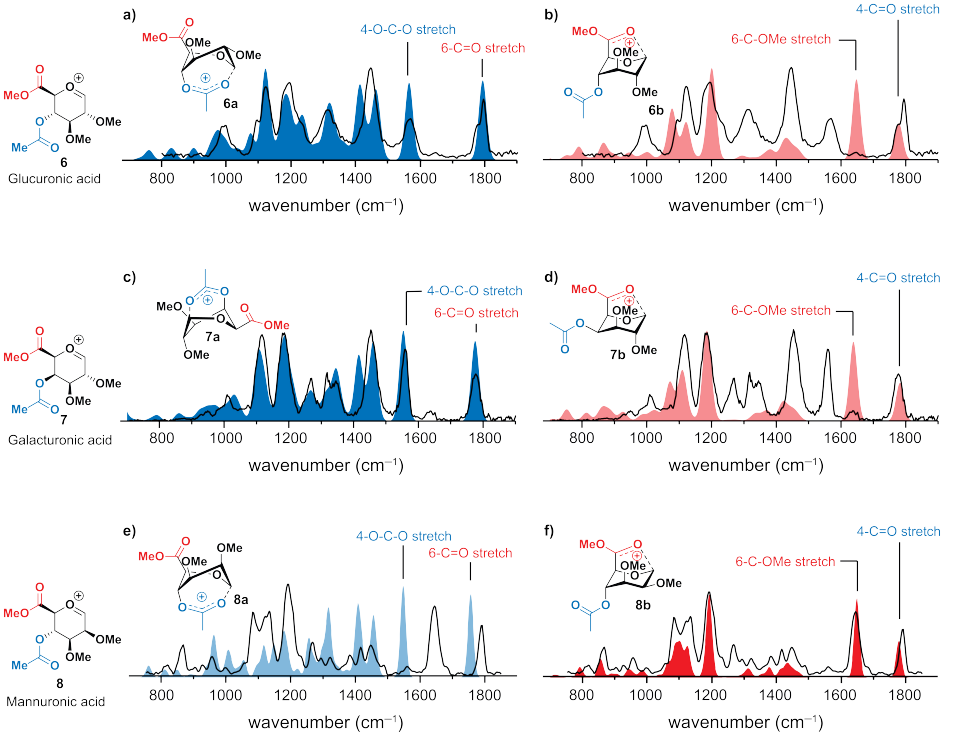

Figure S1. IR ion spectra of uronic acid cations **6**, **7** and **8**. Comparison of the measured IR-ion spectrum (black line) of **6**, **7** and **8** with the calculated spectra (filled) of C-4 (a, c and e in blue) or C-5 (b, d and f in red) stabilization. The assigned major and minor isomers are represented by the full-color and opaque-color spectra, respectively. Panel e and f are adapted from Elferink *et al.*[17]

As was reported previously, the ManA donor ionizes to preferentially provide the C-1,C-5-dioxolanium ion, with the C-1,C-4-dioxepanium ion being present in minor amounts (Figure S1e). For the TalA cation **10**, a strong absorption is observed at 1650 cm^{-1} (Figure S2c and S2d), indicative of the C-1,C-5-dioxolanium ion. The C-1,C-4-dioxepanium ion stretch vibration is also apparent in the spectrum at 1550 cm^{-1}, suggesting the presence of this ion as a minor species. To benchmark the stabilization of the TalA ion, talose donor **5** was ionized, yielding, after CID, the IRIS spectrum shown in Figure S2a,b. The calculated spectrum of the talosyl oxocarbenium gave poor overlap with the recorded spectrum, while the C-1,C-4-dioxepanium ion matched well. This result indicates that formation of the C-1,C-4-dioxepanium ion by the attack of the axial C-4 acetyl group on the anomeric oxocarbenium ion can take place to provide a more stable ion. Thus, while the talosyl ion resembles the galactosyl ion in terms of dioxepanium ion formation and not the mannosyl ion, the TalA ion more closely matches the ManA system and provides the C-1,C-5-dioxolanium ion as the major species. Again, the contribution of the minor species can be estimated by optimizing the weighted average of the computed spectra, which gives contributions of 23 % and 34 % of the C-1,C-4-dioxepanium ion to the total population for ManA and TalA, respectively (see Supporting Figure S4).

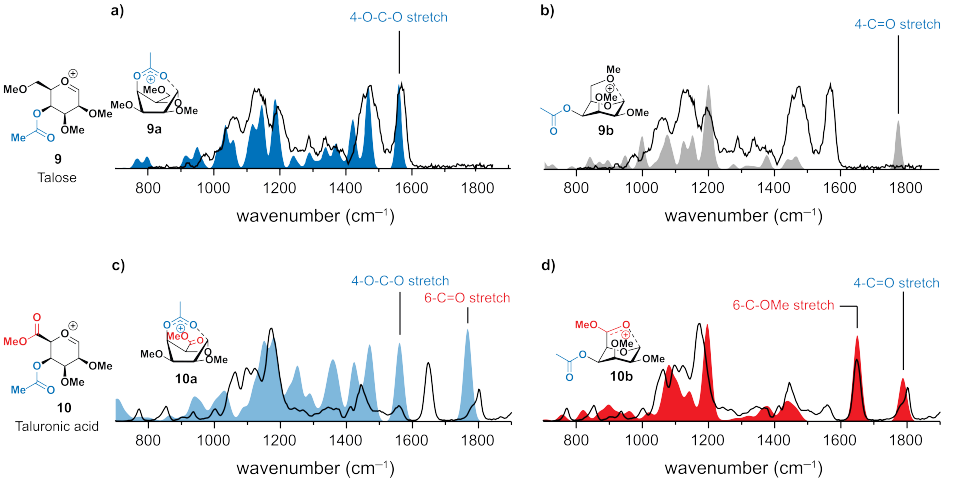

Figure S2. IR ion spectra of talosyl cations **9** and **10**. Comparison of the measured IR-ion spectrum (black line) of **9** and **10** with the calculated spectra (filled) of C-4 (a and c in red) or C-5 (b in gray and d in red) stabilization. The assigned major and minor isomers are represented by the full-color and opaque-color spectra, respectively.

Isomer population analysis

To experimentally determine the relative population of the different cationic species, isomer population analysis was performed (Figure S3). In this experiment, the irradiation occurs at specific IR frequencies, which are diagnostic for one of the isomers. The ion population is irradiated with an increasing number of laser pulses to fragment the absorbing ions.[47,61,62] The normalized precursor depletion ($[1-I_{precursor}/I_{total}]\times100$ %) is plotted as a function of the number of laser pulses to generate an ion depletion curve. When depletion curves do not converge to 100 %, the presence of isomeric structures is indicated, which do not absorb at the selected IR wavelength and whose relative abundance can thus be determined. First, the stability of the isolated glycosyl cations was studied by varying the isolation time. In the case of galacturonic acid **7** and taluronic acid **10**, no significant time-dependent auto-fragmentation was observed. In contrast, mannuronic acid **8** and glucuronic acid cation **6** showed auto-fragmentation over time, and thus could not be used for isomer population analysis.

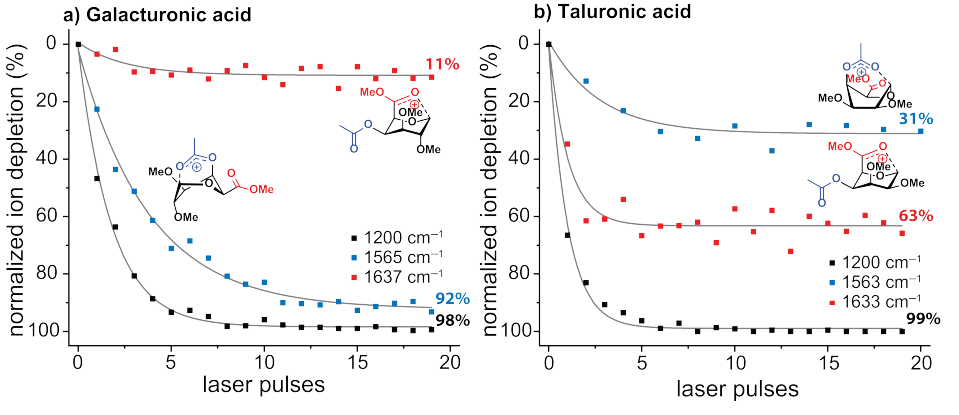

Figure S3. Isomer population analysis of cations **7** and **10**. The laser was set on frequencies characteristic for C-4 participation (blue squares), the C-5 participation (red squares). As control a frequency was used, in which both structures are predicted to absorb (black squares). The experimental data were fitted with a single exponential decay (grey lines). a) Isomer population analysis of cation **7**. b) Isomer population analysis of cation **10**.

The isomer population analysis on the GalA and TalA ions **7** and **10** was performed at approximately 1565 cm^{-1} and approximately 1635 cm^{-1} (diagnostic for C-4 participation and C-5 participation, respectively). As a control experiment, measurements were performed at a frequency where both isomers are predicted to absorb (ca. 1200 cm^{-1}). The control experiments show complete depletion of the parent ion mass, confirming a common frequency region of absorption. Next, the depletion of the C-1,C-4-dioxepanium ion diagnostic peak at ~1565 cm^{-1} was explored. In the case of galacturonic acid **7**, a sharp decrease in ion population was observed, resulting in ~90 % depletion, as determined by the fitted exponential decay (grey line). In line with the computational results, this experiment reveals the C-1,C-4-dioxepanium ion isomer as the major species in the mixture of galacturonic acid cations. In contrast, the ion population of taluronic acid at 1563 cm^{-1} showed a plateau at ~30 % depletion, indicating that the TalA C-1,C-4-dioxepanium ion is not the major species in the ion mixture. Subsequently, the ion populations at ~1635 cm^{-1} (diagnostic for C-5 stabilization) were measured. For galacturonic acid **7** a plateau was reached at around 10 %, which agrees well with the presence of the C-1,C-4-dioxepanium ion in the mixture being approximately 90 %. In the case of the TalA ion **10**, a ~65 % depletion of the ion population was observed, indicating the C-1,C-5-dioxolanium ion to be the major species in the gas-phase ion mixture, which corresponds well with the presence of the C-1,C-4-dioxepanium ion at about 30 % in the mixture, as derived from irradiation at 1563 cm^{-1}. The relative ratio of isomers roughly corresponds to the stability of the ions as established with the CEL computations. The population analyses demonstrate that the contribution of the minor species (11 % and 31 %) is lower than was estimated by mixing of the computational spectra by minimization of the RMS deviation from experiment (20 % and 34 %). The contribution of very minor species might be overestimated by this method as it broadens the mixed computed spectrum, reducing spectral mismatch caused by slight frequency shifts. Of note, the fact that it is possible to selectively deplete the mixture of either component, indicates that under the experimental conditions the C-1,C-4- and C-1,C-5-bridged ions do not equilibrate on the experimental time-scale of 2 seconds (20 laser pulses at 10 Hz). Indeed, the computed reaction profile for the interconversion of both isomers (see Supporting Table S1 and Figure 3), shows a significant barrier (18.4 and 23.5 kcal mol^{-1} for the GalA and TalA, respectively).

Fit of measured IR-spectra with optimized mixtures

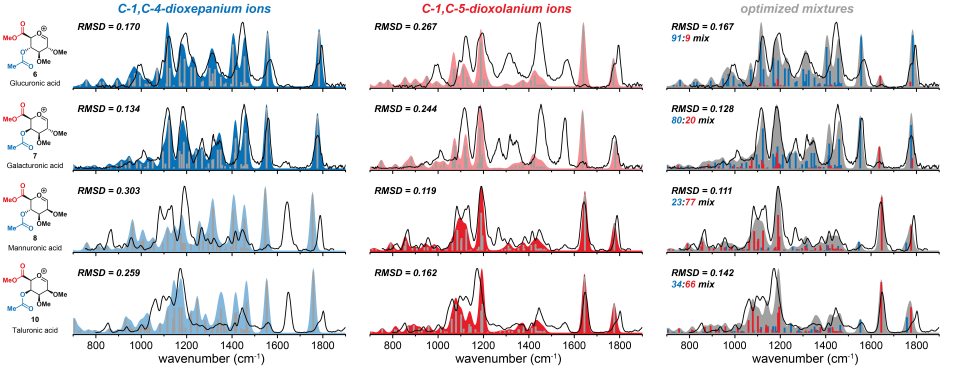

Figure S4. Comparison of the calculated spectra of C-1,C-4-dioxepanium (left column, in blue) and C-1,C-5-dioxolanium (middle column, in red) structures of glycosyl cations **6**, **7**, **8** and **10** with measured spectra (black lines) of m/z=261 CID fragment of compounds **1**, **2**, **3** and **4**, respectively. The right column shows optimized mixtures of the computed spectra, with the ratio inscribed, as derived by the procedure of Barnes *et al.* (also described above).[40] The sticks in the spectra correspond to the fundamental vibrations. Additionally, the root-mean-squared deviation (RMSD) between each computed and experimental spectrum is given.

Match of measured IR-spectra with calculated oxocarbenium and ring-opened structures

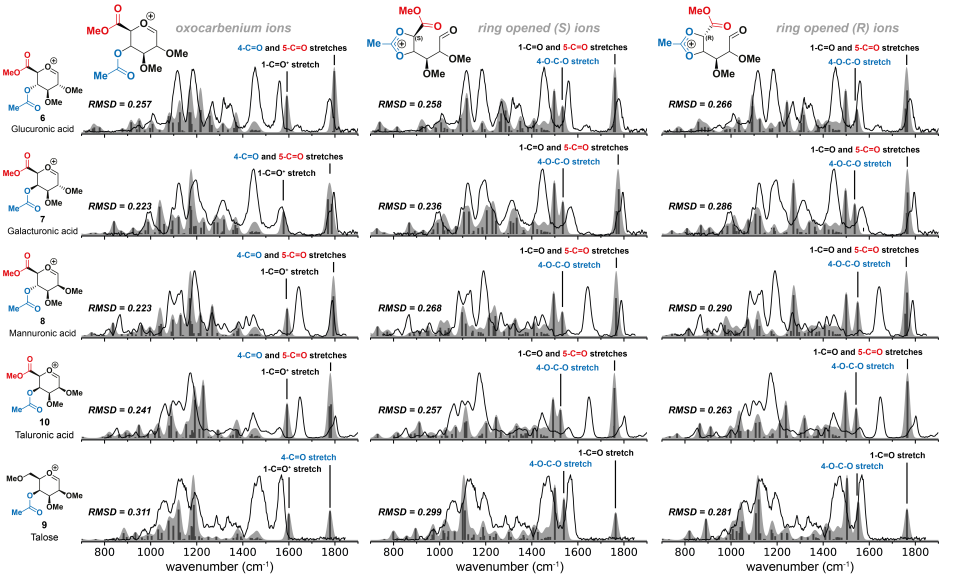

Figure S5. Comparison of the calculated spectra of oxocarbenium ion (left column) and both stereoisomers of the ring-opened ion (middle and right column) structures of glycosyl cations **6**, **7**, **8**, **9** and **10** with measured spectra (black lines) of m/z=261 CID fragment of compounds **1**, **2**, **3**, **5** and **4**, respectively. The sticks in the spectra correspond to the fundamental vibrations. Additionally, the root-mean-squared deviation (RMSD) between each computed and experimental spectrum is given. Key peaks are indicated in the graph.

Supporting computational figures and tables

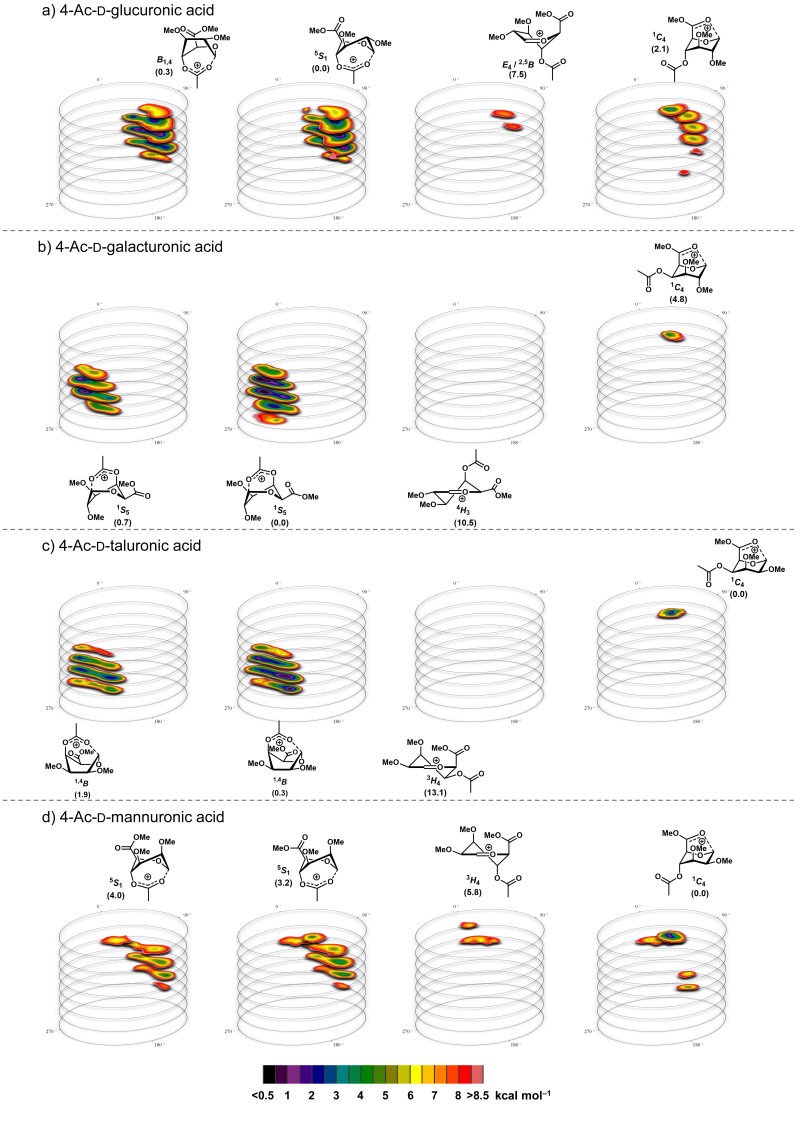

Figure S6. CEL maps of 2,3-OMe-4-OAc-D-glycosyl cations in which the local minima identified are shown with their respective energy. For uronic acids two acetyl ester (R1 and R2) and two methoxy-acid rotamers (eclipsed and bisected) were considered for all computed glycosyl cations generating four separate CEL maps (R1 bisected, R1 eclipsed, R2 bisected, R2 eclipsed). A: CEL maps for glucuronic acid cations, B: CEL maps for galacturonic acid cations, C: CEL maps for taluronic acid cations, D: CEL maps for mannuronic acid cations. All energies are as computed at MP2/6-311++G(2d,2p)//B3LYP/6-311G(d,p) at 298.15 K and expressed as gas-phase Gibbs free energy in kcal mol^{-1}.

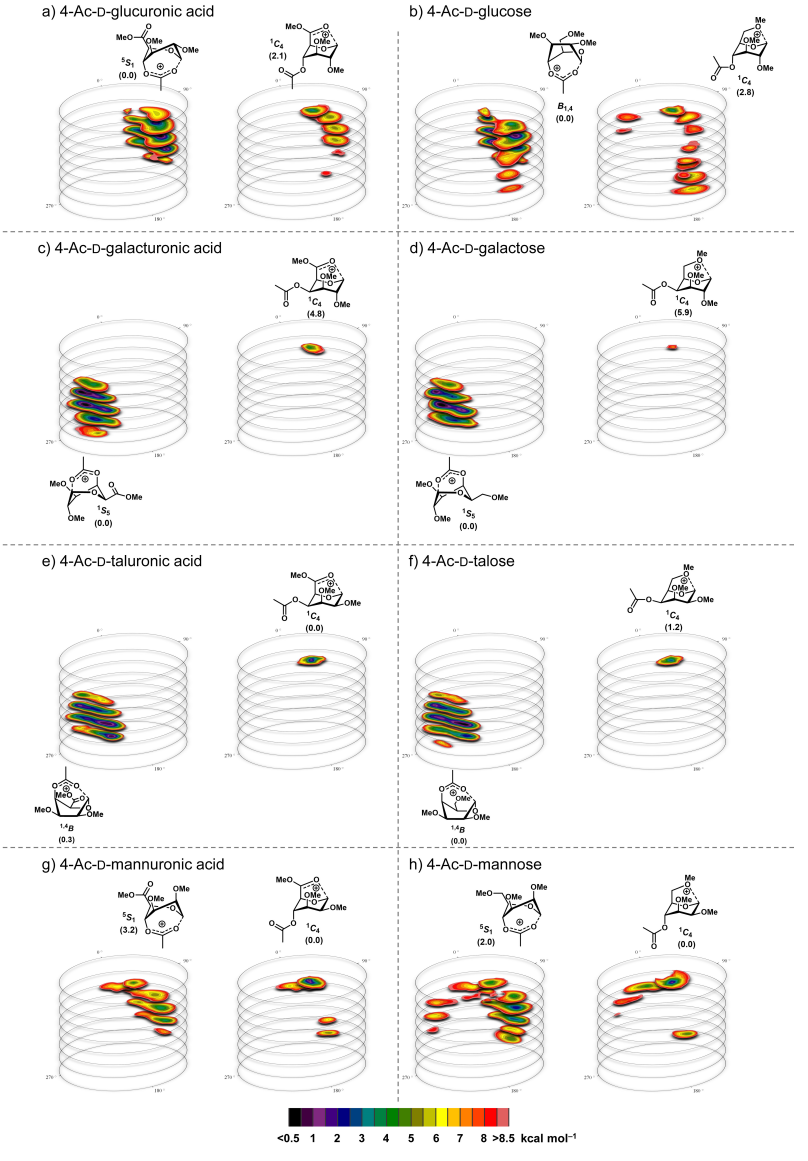

Figure S7. CEL maps of 2,3-OMe-4-OAc-D-glycosyl cations in which the local minima identified are shown with their respective energy. For uronic acids two acetyl ester (R1 and R2) and two methoxy-acid rotamers (eclipsed and bisected) were considered for all computed glycosyl cations generating four separate CEL maps (R1 bisected, R1 eclipsed, R2 bisected, R2 eclipsed). Note, that only eclipsing methoxy-acid rotamers are shown since they are lower in energy than the corresponding biclipsing rotamers. For non-uronic acids two acetyl esters (R1 and R2) and three C-6 orientations (*gt*, *tg*, *gg*) were considered for all computer glycosyl cations. Only the lowest energy C-6 orientation was used to construct the CEL, yielding two separate CEL maps (R1 and R2). All energies are as computed at MP2/6-311++G(2d,2p)//B3LYP/6-311G(d,p) at 298.15 K and expressed as gas-phase Gibbs free energy in kcal mol^{-1}. A: CEL maps for glucuronic acid cations, B: CEL maps for glucose cations. C: CEL maps for galacturonic acid cations, D: CEL maps for galactose cations, E: CEL maps for taluronic acid cations, F: CEL maps for talose cations, G: CEL maps for mannuronic acid cations, H: CEL maps for mannose cations.

Table S1. a) The stationary points examined for 2,3-OMe-4-OAc-D-gluc- and mannuronic acids. b) The stationary points examined for 2,3-OMe-4-OAc-D-galact- and taluronic acid cations. c. Table of the potential energy surfaces (PES) of 2,3-OMe-4-OAc-D-uronic acids. All energies are as computed at MP2/6-311++G(2d,2p)//B3LYP/6-311G(d,p) at 298.15 K and expressed as gas-phase Gibbs free energy in kcal mol^{-1}.

a) Downward O-4 epimers

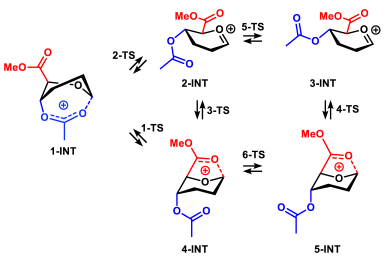

b) Upward O-4 epimers

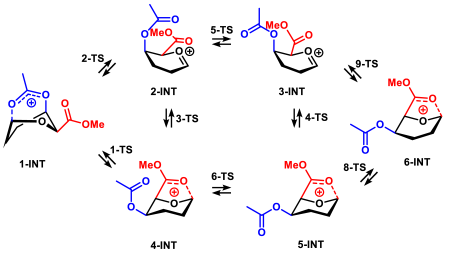

c)

	Glucuronic Acid ΔG (kcal mol^{-1})	Galacturonic Acid ΔG (kcal mol^{-1})	Mannuronic Acid ΔG (kcal mol^{-1})	Taluronic Acid ΔG (kcal mol^{-1})
1-INT	0.0	0.0	6.3	0.5
2-INT	[a]	16.0	9.5	16.8
3-INT	6.1	17.3	8.4	13.1
4-INT	12.1	7.1	5.6	3.6
5-INT	1.2	1.9	0.0	0.0
6-INT	[b]	[b]	[b]	13.1
1-TS	14.3	[c]	13.8	33.9
2-TS	[a]	18.4	11.4	17.6
3-TS	[a]	17.3	[c]	23.5
4-TS	8.5	17.2	11.5	21.4
5-TS	14.2	22.7	15.1	23.5
6-TS	12.7	13.8	6.7	4.5
7-TS	14.4	[a]	[a]	[a]
8-TS	[b]	[b]	[b]	13.8

[a] For glucuronic acid, **2-INT**, **2-TS** and **3-TS** are not a stable stationary points, due to instability of **2-INT**. Instead, **7-TS** dissociates the C-1,C-4-dioxepanium ion through rotation of the C-4 acetate group around the H4-C4-O4-C$_{Acetate}$ bond forming **3-INT**. [b] INT-6 is only a relevant point for taluronic acid due to the steric crowding, resulting in a more complicated conformational change requiring initial deformation to a boat-shaped intermediate **(6-INT)** during formation of the C-1,C-5-dioxolanium ion. [c] The stationary point could not be located.

General synthetic methods

^{1}H and ^{13}C NMR spectra were recorded on a Bruker 400 MHz or 500 MHz spectrometer. Chemical shifts are reported in parts per million (ppm) relative to tetramethylsilane (TMS), or residual solvents as the internal standard. NMR data is presented as follows: chemical shift, multiplicity (s = singlet, d = doublet, t = triplet, dd = doublet of doublets, m = multiplet and/or multiple resonances), coupling constant in hertz (Hz), integration. All NMR signals were assigned on the basis of ^{1}H NMR, ^{13}C NMR, COSY, HSQC and TOCSY experiments. Mass spectra were recorded on an JEOL AccuTOF CS JMST100CS mass spectrometer. Automatic flash column chromatography was performed using Biotage Isolera Spektra One, using SNAP cartridges (Biotage, 30-100 µm, 60 Å), 10-50 g. TLC-analysis was conducted on Silicagel F254 (Merck KGaA) with detection by UV-absorption (254nm) where applicable, and by spraying with 10% sulphuric acid in methanol followed by charring at ≈300 °C. DCM, THF and toluene were freshly distilled. Molecular sieves (4Å) were flame activated under vacuum prior to use. All inert reactions were carried out under argon atmosphere using flame-dried flasks.

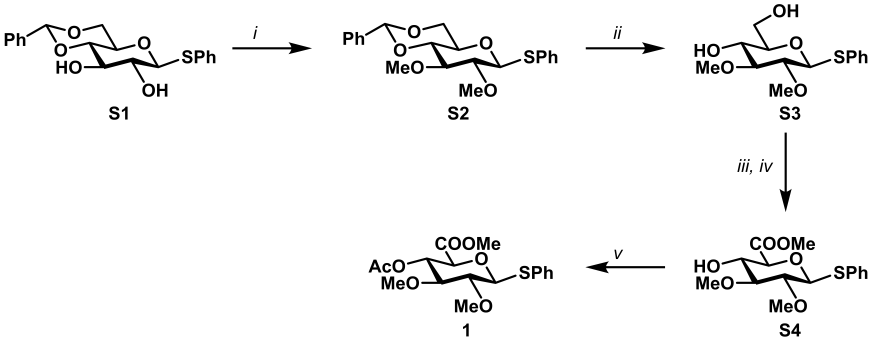

Scheme S1: Synthesis of glucuronic acid derivative and **1**. Reagents and conditions: i) NaH, MeI, DMF, **S2**, 74%; ii) AcOH/H_2O; **S3**, 69%; iii) TEMPO, BAIB, H_2O/DCM; iv) K_2CO_3, MeI, DMF, **S4** 57% over two steps; v) Ac_2O, pyridine; **1**, 76%.

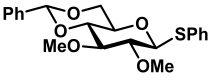

Phenyl 2,3-di-*O*-methyl-4,6-*O*-benzylidene-1-thio-β-D-glucopyranoside (S2). Based on a protocol by Van der Eycken and coworkers.[63] To a solution of **S1** (1.24 g, 3.43 mmol) in THF (25 mL) and DMF (25 mL) sodium hydride (0.41 g, 10.3 mmol, 60 w% in mineral oil) and MeI (0.55 mL, 8.57 mmol) were added at 0 °C, and the solution was stirred at room temperature for 16 h. The reaction mixture was diluted with EtOAc, washed sequentially with water and brine, dried ($MgSO_4$), filtered and concentrated *in vacuo*. The product was purified by recrystallisation from an EtOAc/*n*-heptane to obtain **S2** (984 mg, 74%) as a white solid. TLC: R_f 0.65, (EtOAc/*n*-heptane, 2/3, v/v); ^{1}H NMR (400 MHz, $CDCl_3$): δ = 7.55-7.45 (m, 4H, 4 x C*H* Ar), 7.40-7.26 (m, 6H, 6 x C*H* Ar), 5.54 (s, 1H, C*H* Benzylidene), 4.63 (d, *J* = 9.7 Hz, 1H, H-1), 4.35 (dd, *J* = 10.5, 5.0 Hz, 1H, H-6A), 3.76 (at, *J* = 10.2 Hz, 1H, H-6B), 3.65 (s, 3H, -OC*H*$_3$), 3.64 (s, 3H, -OC*H*$_3$), 3.56 (at, *J* = 9.3 Hz, 1H, H-4), 3.45 (dd, *J* = 9.5, 8.2 Hz, 1H, H-3), 3.42 (td, *J* = 9.7, 5.0 Hz, 1H, H-5), 3.12 (dd, *J* = 9.8, 8.2 Hz, 1H, H-2); ^{13}C NMR (101 MHz, $CDCl_3$): δ = 137.25, 133.05, 132.31, 128.99, 128.97, 128.24, 127.83, 126.06, 101.19, 87.97 (C-1), 84.81 (C-3), 82.24 (C-2), 81.17 (C-4), 70.17 (C-5) , 68.69 (C-6), 61.29, 61.03.

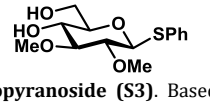

Phenyl 2,3-di-*O*-Methyl-1-thio-β-D-glucopyranoside (S3). Based on a protocol by Chervenak *et al.*[64] A solution of **S2** (496 mg, 1.28 mmol) was stirred in 150 mL 60% aqueous acetic acid at 80 °C for 1 h. The reaction mixture was concentrated *in vacuo* and co-evaporated with toluene. The residue was purified by silicagel column chromatography (0 → 50% EtOAc in *n*-heptane) to afford **S3** (264 mg, 69%) as a white solid. TLC: R_f 0.26, (EtOAc/*n*-heptane, 7/3, v/v); ^{1}H NMR (400 MHz, $CDCl_3$): δ = 7.54-7.46 (m, 2H, 4 x C*H* Ar), 7.35-7.24 (m, 3H, 6 x -CH Ar), 4.63 (d, *J* = 9.6 Hz, 1H, H-1), 3.89 (dd, *J* = 11.8, 3.2 Hz, 1H, H-6A), 3.76 (dd, *J* = 12.2, 5.0 Hz Hz, 1H, H-6B), 3.67 (s, 3H, -OC*H*$_3$), 3.62 (s, 3H, -OC*H*$_3$), 3.50 (at, *J* = 9.3 Hz, 1H, H-4), 3.35 (ddd, *J* = 9.6, 5.2, 3.4 Hz, 1H, H-5), 3.19 (at, *J* = 8.7 Hz, 1H, H-3), 3.12 (dd, J = 9.6, 8.6 Hz, 1H, H-2), 2.65 (bs, 1H, 4-O*H*) 1.65 (bs, 1H, 4-O*H*); ^{13}C NMR (101 MHz, $CDCl_3$): δ = 133.41, 131.76, 129.01, 127.66, 87.86 (C-3), 87.45 (C-1), 82.74 (C-2), 79.03 (C-5), 70.30 (C-4), 62.73 (C-6), 61.19, 60.63.

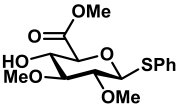

Methyl (phenyl 2,3-di-O-methyl-1-thio-β-D-glucopyranosyl uronate) (S4). Based on a protocol by Zhang *et al.*[65] A solution of **S3** (254 mg, 0.846 mmol) in DCM/*t*-BuOH/H_2O (9 ml, 4/4/1,v/v/v) was cooled to 0 °C and treated with TEMPO and BAIB . After stirring 16 h at 4 °C, sat. aq. $Na_2S_2O_3$ was added and the mixture was stirred for 30 min. It was then diluted with EtOAc and washed with sat. aq. NaCl with a drop of 1 M HCl. The organic phase was dried over Na_2SO_4 and concentrated in vacuo. Toluene was added and evaporated thrice. The crude residue was dissolved in DMF (20 ml), followed by the addition of K_2CO_3 and MeI at 0 °C. The mixture was allowed to stir 16 h at 4 °C, and diluted with EtOAc, washed with sat. aq. NaCl and the organic phase was dried over Na_2SO_4, filtered and concentrated in vacuo. The residue was purified by silicagel column chromatography (60% EtOAc in *n*-heptane) to afford **S4** (158 mg, 57 %) as a yellow oil. TLC: R_f 0.71, (EtOAc/*n*-heptane, 4/1, v/v); ^{1}H NMR (400 MHz, $CDCl_3$): δ = 7.58-7.53 (m, 2H, 2 x -CH Ar), 7.34-7.27 (m, 3H, 3 x -CH Ar), 4.57 (d, J = 9.7 Hz, 1H, H-1), 3.85-3.73 (m, 5H, H-4, H-5, -$COOCH_3$), 3.67 (s, 3H, -OCH_3), 3.61 (s, 3H, -OCH_3), 3.23 (at, J = 8.4 Hz, 1H, H-3), 3.09 (dd, J = 9.7, 8.6 Hz, 1H, H-2), 3.04 (bs, 1H, 4-OH); ^{13}C NMR (101 MHz, $CDCl_3$): δ = 169.59 (C-6), 133.15, 132.25, 128.94, 127.82, 88.14 (C-1), 86.94 (C-3), 81.68 (C-2), 77.43 (C-5), 71.46 (C-4), 61.26, 60.84, 60.48, 52.80. HRMS (m/z): $[M+Na]^+$ calcd for $C_{15}H_{20}O_6S$, 351.0878 found, 351.0886.

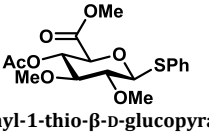

Methyl (phenyl 4-*O*-acetyl-2,3-di-*O*-methyl-1-thio-β-D-glucopyranosyl uronate) (1). To a solution of **S4** (70 mg, 0.21 mmol) in pyridine (1.0 ml) Ac_2O (1.0 ml) and DMAP (2.6 mg, 0.021 mmol) were added. The mixture was stirred for 16 h at room temperature after which it was concentrated *in vacuo*. Purification of the residue by column chromatography (silica gel, pentane/EtOAc, 3/1, v/v) of the residue yielded the product **1** (60 mg, 76%) as a white solid. TLC: R_f 0.61, (EtOAc/*n*-heptane, 1/1, v/v); ^{1}H NMR (400 MHz, $CDCl_3$): δ = 7.59-7.55 (m, 2H, 2 x -C*H* Ar), 7.34-7.28 (m, 3H, 3 x -C*H* Ar), 5.02 (at, *J* = 9.7 Hz, 1H, H-4), 4.52 (d, *J* = 9.8 Hz, 1H, H-1), 3.88 (d, *J* = 9.9 Hz, 1H, H-5), 3.74 (s, 3H, -COOC*H*$_3$), 3.59 (s, 3H, -OC*H*$_3$), 3.55 (s, 3H, -OC*H*$_3$), 3.35 (d, J = 9.5, 8.6 Hz, 1H, H-3), 3.15 (dd, J = 9.7, 8.8 Hz, 1H, H-2), 2.08 (s, 3H, C*H*$_3$ Ac); ^{13}C NMR (101 MHz, $CDCl_3$): δ = 169.59, 167.61 (C-6), 132.74, 132.54, 128.99, 128.03, 87.55 (C-1), 85.18 (C-3), 81.34 (C-2), 76.26 (C-5), 70.92 (C-4), 60.96, 60.92, 52.75, 20.73 ; HRMS (m/z): $[M+Na]^+$ calcd for $C_{17}H_{22}O_7S$, 393.0978; found, 393.0984.

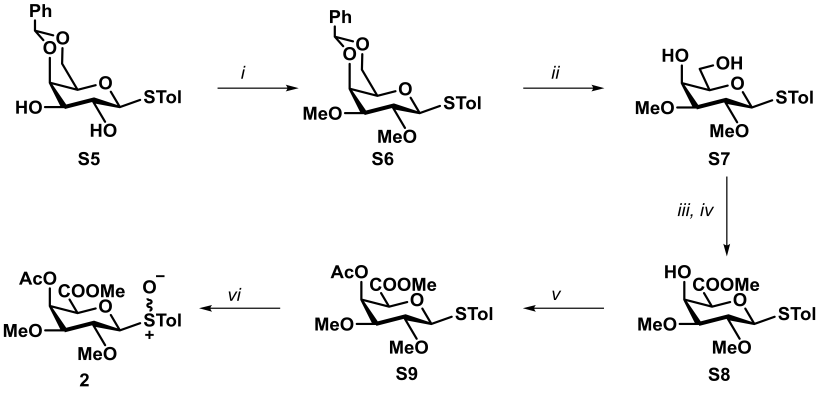

Scheme S2: Synthesis of galacturonic acid derivative **2**. Reagents and conditions: i) NaH, MeI, DMF, **S6**, 91%; ii) AcOH/H_2O; **S7**, 96%; iii) TEMPO, BAIB, H_2O/DCM; iv) K_2CO_3, MeI, DMF, **S8** 93% over two steps; v) Ac_2O, pyridine; **S9**, quant; vi) *m*-CPBA, DCM, **2**, quant.

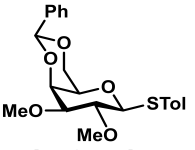

Tolyl 2,3-di-*O*-methyl-4,6-*O*-benzylidene-1-thio-β-D-galactopyranoside (S6). To a mixture tolyl 4,6-*O*-benzylidene-1-thio-β-D-galactopyranoside (**S5**, 1.0 g, 2.8 mmol) in THF/DMF (16 mL, 1/1, v/v) NaH (333 mg, 6.3 mmol, 60 w% in mineral oil) was added. After stirring for 10 minutes, MeI (0.4 ml, 6.9 mmol) was added and the reaction was stirred overnight at rt. The mixture was quenched by addition of sat. aq. NH_4Cl and diluted with EtOAc (30 mL). The resulting emulsion was transferred to a separation funnel and washed with H_2O (30 mL) and brine (30 mL). The organic layer was dried ($MgSO_4$), filtered and concentrated *in vacuo*. Crystallization from EtOAc/*n*-heptane afforded **S6** (980 mg, 91%) as a white solid. TLC: R_f 0.13, (3/7, EtOAc/heptane, v/v); ^{1}H NMR (500 MHz, Chloroform-*d*) δ 7.63 – 7.58 (m, 2H, 2 x C*H* Ar), 7.51 – 7.44 (m, 2H, 2 x C*H* Ar), 7.39 – 7.32 (m, 3H, 3 x C*H* Ar), 7.07 – 7.01 (m, 2H, 2 x C*H* Ar), 5.51 (s, 1H, C*H* benzylidene), 4.46 (d, *J* = 9.4 Hz, 1H, H-1), 4.37 (dd, *J* = 12.3, 1.7 Hz, 1H, H-6A), 4.28 (dd, *J* = 3.5, 1.1 Hz, 1H, H-4), 4.02 (dd, *J* = 12.4, 1.7 Hz, 1H, H-6B), 3.53 (s, 3H, -OCH_3), 3.49 (s, 3H, -OCH_3), 3.46 (t, *J* = 9.4 Hz, 1H, H-2), 3.43 (q, *J* = 1.6 Hz, 1H, H-5), 3.31 (dd, *J* = 9.2, 3.4 Hz, 1H, H-3), 2.32 (s, 3H, CH_3 STol). ^{13}C NMR (126 MHz, Chloroform-*d*) δ 137.92, 137.83, 133.77, 129.67, 129.20, 128.56, 128.23, 126.85, 101.61, 86.59 (C-1), 83.66 (C-3), 76.93 (C-2), 73.21 (C-4), 69.87 (C-5), 69.60 (C-6), 61.01, 57.87, 21.29; HRMS *(m/z)*: $[M+Na]^+$ calcd for $C_{22}H_{26}O_5S$, 425.1399; found, 425.1395.

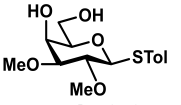

Tolyl 2,3-di-*O*-methyl-1-thio-β-D-galactopyranoside (S7). Tolyl 4,6-benzylidene-2,3-di-*O*-methyl-1-thio-galactopyranoside (**S6**) (800 mg, 1.99 mmol) was dissolved in 80% acetic acid (20 mL, aqueous) and refluxed for 1 hour. After TLC indicated conversion, the mixture was concentrated *in vacuo*. Silica column chromatography (EtOAc/*n*-heptane, 1/4, v/v) of the residue gave **S7** (602 mg, 96 %) as a white solid. TLC: R_f 0.12, (3/7, EtOAc/heptane, v/v); ^{1}H NMR (500 MHz, Acetone-*d*) δ 7.47 – 7.36 (m, 2H, 2 x C*H* Ar), 7.19 – 7.00 (m, 2H, 2 x C*H* Ar), 4.52 (d, *J* = 9.1 Hz, 1H, H-1), 4.16 (ddt, *J* = 4.3, 2.9, 1.3 Hz, 1H, H-4), 3.88 – 3.71 (m, 2H, H-6A, H-6B), 3.67 (dd, *J* = 3.6, 0.9 Hz, 1H, 4-O*H*) 3.51 (td, *J* = 5.9, 1.1 Hz, 1H, H-5), 3.47 (s, 3H, -OCH_3), 3.42 (s, 3H, -OCH_3), 3.35 – 3.21 (m, 2H, H-2, H-3), 2.29 (s, 3H, CH_3 STol); ^{13}C NMR (126 MHz, Acetone-*d*) δ 137.53, 132.14, 130.33, 130.25, 88.23 (C-1), 85.83 (C-3), 79.70 (C-5), 79.48(C-2), 66.10 (C-4), 66.00 (C-4), 62.42 (C-6), 62.29 (C-6), 60.88, 57.04, 21.00; HRMS *(m/z)*: $[M+Na]^+$ calcd for $C_{15}H_{22}O_5S$, 337.1086; found, 337.1098

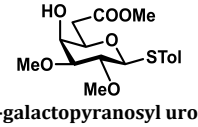

Methyl (tolyl 2,3-di-*O*-methyl-1-thio-β-D-galactopyranosyl uronate) (S8). Based on a protocol by Zhang *et al.* **S7** (602 mg, 1.91 mmol) was dissolved in a mixture of H_2O and DCM (10 mL, 1/9, v/v). To the solution BAIB (1.23 g, 3.83 mmol) and TEMPO (60 mg, 0.38 mmol) were added. The mixture was left under vigorous stirring for two hours before being quenched by 10 % aqueous $Na_2S_2O_3$ solution (10 mL). The mixture was acidified to pH 3 and extracted with EtOAc (3 x 30 mL). The organic layers were combined, dried (MgSO4), filtered and concentrated in vacuo. Silica column chromatography (0 → 15 % MeOH in a mixture of 2 % AcOH in DCM) gave the product (629 mg, quant.) as an amorphous white solid which was dissolved in DMF. To the solution, K_2CO_3 (265 mg, 1.92 mmol) and MeI (240 µL, 3.83 mmol) were added. The mixture for two hours to completion and was diluted with EtOAc (50 mL) and washed with sat. aq. NaCl (40 mL). The organic layer was dried (MgSO4), filtered and concentrated in vacuo. Silica column chromatography of the residue (0 → 60% EtOAc in *n*-heptane) gave **S8** (610 mg, 93%) as a clear oil. TLC: R_f 0.31, (3/2, EtOAc/heptane, v/v); ^{1}H NMR (400 MHz, Acetone-*d6*) δ 7.67 – 7.44 (m, 2H, 2 x C*H* Ar), 7.20 – 7.01 (m, 2H, 2 x C*H* Ar), 4.46 – 4.35 (m, 2H, H-1, H-4), 4.04 (t, *J* = 1.2 Hz, 1H, H-5), 3.83 (s, 3H, COOCH_3), 3.58 (s, 3H, -OCH_3), 3.51 (s, 3H, -OCH_3), 3.37 – 3.23 (m, 2H, H-3, H-4), 2.36 (dd, *J* = 3.6, 1.1 Hz, 1H, 4-O*H*), 2.32 (s, 3H, CH_3 STol); ^{13}C NMR (101 MHz, Acetone-*d6*) δ 168.41 (C-6), 138.29, 133.69, 129.78, 87.82 (C-1), 84.22 (C-3), 78.01 (C-2), 77.01 (C-5), 67.22 (C-4), 61.37, 57.86, 52.76, 21.29; HRMS *(m/z)*: $[M+Na]^+$ calcd for $C_{15}H_{22}O_5S$, 365.1035; found, 365.1032.

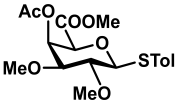

Methyl (tolyl 4-*O*-acetyl-2,3-di-O-methyl-1-thio-β-D-galactopyranosyl uronate) (S9). S8 (50 mg, 0.15 mmol) was dissolved in pyridine (1.0 mL). Acetic anhydride (0.50 mL, 5.29 mmol) and DMAP (4.5 mg, 0.037 mmol) were added and the reaction stirred for 1 hour at rt. The solution was concentrated *in vacuo* and coevaporated three times with toluene (5.0 mL). The residue was diluted with EtOAc (10 mL) and washed with 1.0 M aqueous HCl (10 mL), H_2O (10 mL) and brine (10 mL). The organic layer was dried ($MgSO_4$), filtered and concentrated *in vacuo*. The product **S9** (56 mg, quant.) was obtained as a clear oil. TLC: R_f 0.42, (1/1, EtOAc/*n*-heptane, v/v); ^{1}H NMR (400 MHz, Chloroform-*d*) δ 7.59 – 7.51 (m, 2H, 2 x C*H* Ar), 7.14 – 7.08 (m, 2H, 2 x C*H* Ar), 5.70 (dd, *J* = 3.2, 1.2 Hz, 1H, H-4), 4.45 (d, *J* = 9.2 Hz, 1H, H-1), 4.11 (d, *J* = 1.2 Hz, 1H, H-5), 3.75 (s, 3H, COOCH_3), 3.57 (s, 3H, -OCH_3), 3.43 (s, 3H, -OCH_3), 3.32 (dd, *J* = 9.0, 3.2 Hz, 1H, H-3), 3.26 (t, *J* = 9.2 Hz, 1H, H-2), 2.32 (s, 3H, CH_3 STol), 2.07 (s, 3H, CH_3 Acetyl); ^{13}C NMR (101 MHz, Chloroform-*d*) δ 170.05, 167.28 (C-6), 138.24, 133.64, 129.68, 129.19, 88.01 (C-1), 83.17 (C-3), 77.86 (C-2), 75.72 (C-5), 67.32 (C-4), 61.43, 58.10, 52.72, 21.28, 20.85; HRMS *(m/z)*: $[M+Na]^+$ calcd for $C_{18}H_{24}O_5S$, 407.1140; found, 407.1144.

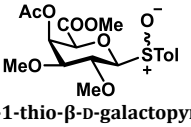

Methyl (tolyl 4-*O*-acetyl-2,3-di-O-methyl-1-thio-β-D-galactopyranosyl uronate) *S*-oxide (2). Based on a protocol by Gómez *et al.* A solution of **S9** (13 mg, 0.034 mmol) in DCM (0.77 mL) was cooled to –78 °C under inert atmosphere and then *m*-CPBA (8.8 mg, 0.036 mmol) was added. The reaction was stirred for three hours, diluted with DCM (15 mL) and washed with 10% aq. $Na_2S_2O_3$ solution, sat. aq. $NaHCO_3$ and brine. The organic layer was dried ($MgSO_4$), filtered, concentrated *in vacuo*. The crude product **2** (14 mg) was used directly for IRMPD experiments. HRMS *(m/z)*: $[M+Na]^+$ calcd for $C_{18}H_{24}O_8S$, 423.1090; found, 423.1095.

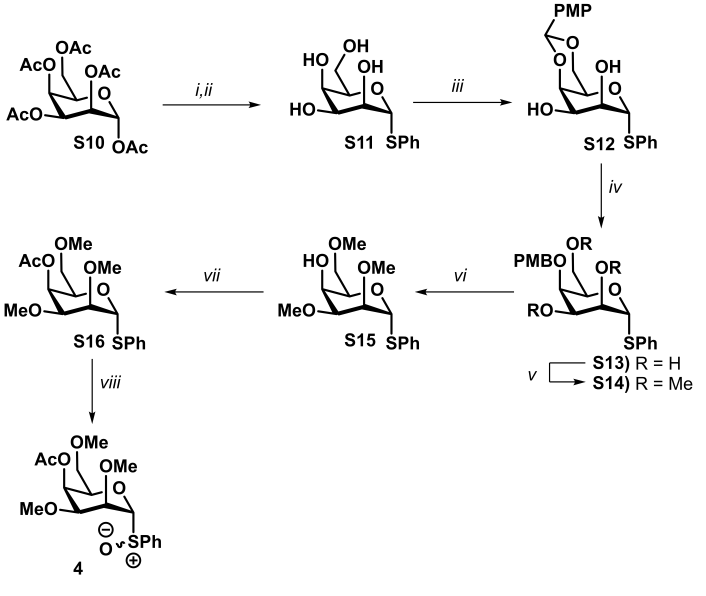

Scheme S3. *i*) thiophenol, $BF_3.Et_2O$, DCM; *ii*) K_2CO_3, MeOH; **S11**, 75% over two steps; *iii*) anisaldehyde dimethyl acetal, HBF_4, DMF; **S12**, 79%; *iv*) $BH_3.Et_2O$, TMSOTf, THF; **S13**, 60%; *v*) MeI, NaH, DMF; **S14**, 96%; *vi*) *p*TsOH, MeOH; **S15**, 93%; *vii*) Ac_2O, pyridine; **S16**, quant; *viii*) *m*-CPBA, DCM; **4**, used as crude for IRIS.

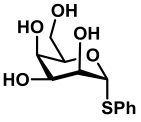

Phenyl 1-thio-α-D-talopyranoside (S11). To a solution of 1,2,3,4,6-penta-*O*-acetyl-α-D-talopyranoside[37] (**S10**, 1.2 g, 3.1 mmol) in dry DCM (15 mL) under inert atmosphere at rt, thiophenol (0.48 mL, 4.6) and boron trifluoride diethyl etherate (1.9 mL, 15 mmol) were added. The mixture was stirred for 18 min after which it was poured out in sat. aq. $NaHCO_3$ (50 ml) under vigorous stirring. The organic layer was collected and washed with 5% aq. NaOH (2 x 20 mL) and brine (20 mL). The aqueous layers were extracted with DCM (5 mL) and the combined organic layers were dried ($MgSO_4$), filtered and concentrated *in vacuo*. Silicagel flash column chromatography (0% → 60% EtOAc in *n*-heptane) of the residue afforded phenyl 2,3,4,6-tetra-*O*-acetyl-1-thio-α-D-talopyranoside (1.1 g, 81%) as a white solid (**TLC**: (EtOAc/*n*-heptane, 50/50 v/v): R_f 0.41) and was used directly in the synthesis of **S11**. To a stirred solution of phenyl 2,3,4,6-tetra-*O*-acetyl-1-thio-α-D-talopyranoside[66] (1.0 g, 2.3 mmol) in MeOH (7.6 mL), K_2CO_3 (31 mg, 0.23 mmol) was added. The mixture was stirred for 1 h and neutralized by addition of Dowex (H^+) resin. After filtration, the solution was concentrated *in vacuo* to afford **S11** (570 mg, 92%) as a clear oil. TLC: R_f 0.08, (EtOAc/*n*-heptane, 83/17, v/v); ^{1}H NMR (500 MHz, Methanol-d_4) δ 7.56 – 7.53 (m, 2H, C*H* Ar), 7.33 – 7.28 (m, 3H, C*H* Ar), 5.51 (d, *J* = 1.5 Hz, 1H, H-1), 4.28 (td, *J* = 6.2, 1.3 Hz, 1H, H-5), 4.03 – 4.02 (m, 1H, H-4), 3.92 – 3.91 (m, 1H, H-2), 3.79 – 3.74 (m, 2H, H-6A, H-6B), 3.71 (t, *J* = 3.2 Hz, 1H, H-3). ^{13}C NMR (126 MHz, MeOD) δ 134.26, 131.69, 129.65, 128.69, 128.58, 127.20, 126.40, 89.63 (C-1), 88.26, 79.87, 73.18, 72.84 (C-4), 72.66 (C-5), 70.25 (C-2), 66.50 (C-3), 61.20 (C-6).

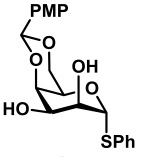

Phenyl 4,6-*O*-*p*-methoxybenzylidene-1-thio-α-D-talopyranoside (S12). To a solution of phenyl 1-thio-α-D-talopyranoside **(S11)** (130 mg, 0.477 mmol) in anhydrous DMF (2.39 mL), were added while stirring under inert atmosphere at 0 °C: anisaldehyde dimethyl acetal (86 µL, 0.501 mmol) and tetrafluoroboric acid diethyl etherate complex (62.2 µL, 0.454 mmol). After 72 h of stirring the reaction was quenched with TEA (100 µL) and concentrated *in vacuo*. Crystallization from pure ethanol gave the product **S12** (95 mg, 51%) as colorless crystals. Silicagel flash column chromatography (40 % → 50 % EtOAc in *n*-heptane) of the residue afforded additional **S12** (52 mg, 28%) as a white solid. TLC: R_f 0.40, (EtOAc/*n*-heptane, 2/3 v/v); ^{1}H NMR (500 MHz, $CDCl_3$) δ 7.55 – 7.47 (m, 2H, 2 x C*H* Ar), 7.42 (d, *J* = 8.7 Hz, 2H, 2 x C*H* Ar), 7.34 (at, *J* = 7.4 Hz, 2H, 2 x C*H* Ar), 7.31 – 7.26 (m, 1H, C*H* Ar), 6.92 (d, *J* = 8.7 Hz, 1H, 2 x C*H* Ar), 5.80 (s, 1H, H-1), 5.50 (s, 1H, C*H* PMP acetal), 4.38 – 4.26 (m, 2H, H-6A, H-4), 4.22 (bs, 1H, H-5), 4.12 (dd, *J* = 12.7, 1.6 Hz, 1H, H-6B), 4.08 – 3.99 (m, 1H, H-2), 3.92 (bs, 1H, H-3), 3.82 (s, 3H, OCH_3) 3.60 (d, *J* = 12.1 Hz, 1H, 2-O*H*), 3.07 (d, *J* = 9.5 Hz, 1H, 3-O*H*); ^{13}C NMR (126 MHz, $CDCl_3$) δ 160.47, 133.93, 130.89, 129.69, 129.28, 127.50, 127.46, 113.89, 101.85, 89.07 (C-1), 76.77 (C-4), 71.74 (C-2), 69.69 (C-6), 66.29 (C-3), 63.85 (C-5), 55.42; HRMS *(m/z)*: $[M+Na]^+$ calcd for $C_{20}H_{22}O_6S$, 413.1035; found, 413.1035.

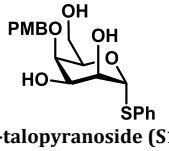

Phenyl 4-*O*-(*p*-methoxybenzyl)-1-thio-α-D-talopyranoside (S13). To a mixture of **S12** (86 mg, 0.22 mmol) in DCM (2.2 mL), BH_3.THF (1.5 mL, 1.0 M in THF) was added at 0 °C under inert atmosphere. Next, TMSOTf (4.0 µL, 22 µmol) was added and the reaction stirred for 1 hour to completion. The mixture was neutralized by addition of triethylamine (3 drops) and carefully quenched by addition of methanol. The solution was concentrated *in vacuo* and the residue purified by silica column chromatography (40→ 50 % EtOAc in *n*-heptane). The product **S13** (52 mg, 60 %) was obtained as a colorless oil. **TLC**: R_f 0.18, (EtOAc/*n*-heptane, 2/3 v/v); ^{1}H NMR (400 MHz, MeOD) δ 7.56 – 7.49 (m, 2H, 2 x C*H* PMB), 7.37 – 7.23 (m, 5H, 5 x C*H* Ar), 6.94 – 6.84 (m, 2H, 2 x C*H* PMB), 5.44 (d, *J* = 1.3 Hz, 1H, H-1), 4.89 (d, *J* = 10.4 Hz, 1H, C*H*H PMB), 4.57 (d, *J* = 10.4 Hz, 1H, C*H*H PMB), 4.31 (t, *J* = 6.4 Hz, 1H H-5), 3.96 – 3.92 (m, 2H, H-2, H-4), 3.88 (t, *J* = 3.1 Hz, 1H, H-3), 3.78 (s, 3H, -OCH_3 PMB), 3.72 – 3.58 (m, 2H, H-6A, H-6B); ^{13}C NMR (126 MHz, MeOD) δ 159.70, 134.16, 131.72, 130.04, 129.67, 129.06, 128.66, 127.96, 127.20, 113.42, 89.67 (C-1), 77.50 (C-4), 75.15 (CH_2, PMB), 73.07 (C-2), 72.31 (C-5), 67.26 (C-3), 61.24 (C-6), 60.63 (OCH_3, PMB); HRMS *(m/z)*: $[M+Na]^+$ calcd for $C_{20}H_{24}O_6S$, 415.1191; found, 415.1200.

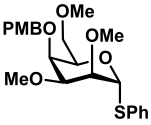

henyl 2,3,6-tri-*O*-methyl-4-*O*-*p*-methoxybenzyl-1-thio-α-D-talopyranoside (S14). To a mixture of **S13** (45 mg, 0.11 mmol) in DMF, MeI (37 µL, 0.57 mmol) and NaH (28 mg, 60 w% in mineral oi) was added at 0 °C. The mixture stirred for two hours before being quenched by the addition of sat. aq. NH_4Cl. The mixture was diluted with Et_2O (15 mL) and washed with 5% aq. LiCl (5 mL) and brine (5 mL). The organic layer was dried ($MgSO_4$), filtered and concentrated *in vacuo*. The residue was purified by silica column chromatography to give **S14** (48 mg, 96%) as amorphous solid. TLC: R_f 0.33, (EtOAc/*n*-heptane, 2/3, v/v); ^{1}H NMR (500 MHz, $CDCl_3$) δ 7.50 (dd, *J* = 8.3, 1.2 Hz, 2H, C*H* PMB), 7.34 – 7.21 (m, 5H, 5 x C*H* Ar), 6.89 – 6.83 (m, 2H, 2 x C*H* PMB), 5.70 (d, *J* = 2.0 Hz, 1H, H-1), 4.81 (d, *J* = 11.8 Hz, 1H, C*H*H PMB), 4.62 (d, *J* = 11.8 Hz, 1H, C*H*H PMB), 4.33 (td, *J* = 6.2, 2.0 Hz, 1H, H-5), 3.84 (t, *J* = 2.0 Hz, 1H, H-4), 3.80 (s, 3H, OC*H*$_3$ PMB), 3.70 (ad, *J* = 2.4 Hz, 1H, H-2), 3.56 (dd, *J* = 10.2, 6.6 Hz, 1H, H-6A), 3.54 – 3.46 (m, 8H, 2 x OC*H*$_3$, H-3, H-6B), 3.24 (s, 3H, OC*H*$_3$); ^{13}C NMR (126 MHz, $CDCl_3$) δ 159.30, 134.62, 131.14, 130.99, 130.10, 129.11, 127.28, 113.70, 84.82 (C-1), 79.17 (C-3), 79.09 (C-2), 73.29 (*C*H$_2$, PMB), 71.99 (C-4), 71.89 (C-5), 71.32 (C-6), 59.26, 59.17, 57.55, 55.42 (O*C*H$_3$, PMB); HRMS *(m/z)*: $[M+Na]^+$ calcd for $C_{23}H_{30}O_6S$, 457.1661; found, 457.1660.

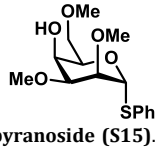

Phenyl 2,3,6-tri-*O*-methyl-1-thio-α-D-talopyranoside (S15). To a suspension of **S14** (40 mg, 92 µmol) in MeOH (1.0 mL), pTsOH (18 mg, 92 µmol) was added. The mixture stirred at 50 °C for 2 hours to completion. The reaction was quenched by addition of a drop of TEA and concentrated *in vacuo*. The residue was purified by silicagel column chromatography (40→50% EtOAc in *n*-heptane) to obtain the product **S15** (27 mg, 93%) as a amorphous solid. TLC: R_f 0.25, (EtOAc/*n*-heptane, 1/1, v/v):; ^{1}H NMR (500 MHz, $CDCl_3$) δ 7.60 – 7.49 (m, 2H, 2 x C*H* Ar), 7.32 (adddd, *J* = 12.1, 6.9, 4.6, 2.1 Hz, 3H, 3 x C*H* Ar), 5.67 (d, *J* = 1.1 Hz, 1H, H-1), 4.38 (t, *J* = 6.1 Hz, 1H, H-5), 4.06 – 3.98 (m, 1H, H-4), 3.86 (dt, *J* = 2.8, 1.4 Hz, 1H, H-2), 3.74 (dd, *J* = 10.1, 5.3 Hz, 1H, H-6A), 3.67 (dd, *J* = 10.1, 6.8 Hz, 1H, H-6B), 3.50 (s, 6H, 2 x OCH_3), 3.44 (add, *J* = 6.2, 3.1 Hz, 2H, H-3, 4-O*H*), 3.38 (s, 3H, OCH_3); ^{13}C NMR (126 MHz, $CDCl_3$) δ 133.91, 131.84, 129.12, 127.75, 85.26 (C-1), 80.34 (C-2), 75.76 (C-3), 71.85 (C-6), 71.65 (C-5), 67.02 (C-4), 59.27, 58.82, 55.79; HRMS *(m/z)*: $[M+Na]^+$ calcd for $C_{15}H_{22}O_5S$, 337.1086; found, 337.1083.

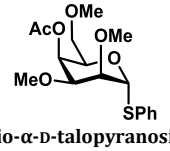

Phenyl 4-*O*-acetyl-2,3,6-tri-*O*-methyl-1-thio-α-D-talopyranoside (S16). **S14** (2 mg, 6 µmol) was dissolved in pyridine (1.0 mL). Acetic anhydride (0.50 mL, 5.29 mmol) and DMAP (4.5 mg, 0.037 mmol) were added and the reaction stirred for 5 hours at rt. The solution was concentrated *in vacuo* and coevaporated three times with toluene (5.0 mL). The residue was diluted with EtOAc (10 mL) and washed with 1.0 M aqueous HCl (10 mL), H_2O (10 mL) and brine (10 mL). The organic layer was dried ($MgSO_4$), filtered and concentrated *in vacuo*. Silicagel column chromatography of the residue (50% EtOAc in *n*-heptane) gave the product **S16** (2 mg, quant.) as a clear oil. TLC: R_f 0.42, (1/1, EtOAc/*n*-heptane), v/v; TLC: (EtOAc/*n*-heptane, 2/3, v/v): R_f 0.24; ^{1}H NMR (500 MHz, $CDCl_3$) δ 7.55 – 7.49 (m, 2H, 2 x C*H* Ar), 7.35 – 7.29 (m, 2H, 2 x C*H* Ar), 7.29 – 7.23 (m, 1H, 1 x C*H* Ar), 5.76 (d, *J* = 1.1 Hz, 1H, H-1), 5.51 (d, *J* = 3.4 Hz, 1H, H-4), 4.55 (td, *J* = 6.0, 1.5 Hz, 1H, H-5), 3.72 (dt, *J* = 3.6, 1.0 Hz, 1H, H-2), 3.58 – 3.48 (m, 4H, H-3, H-6A, H-6B, OC*H*$_3$), 3.47 (s, 3H, OCH_3), 3.30 (s, 3H, OCH_3), 2.17 (d, *J* = 0.6 Hz, 4H, CH_3 Ac, acetone); ^{13}C NMR (126 MHz, $CDCl_3$) δ 170.84, 134.15, 131.20, 129.24, 127.57, 85.53 (C-1), 79.09 (C-2), 76.17 (C-3), 71.21 (C-6), 69.62 (C-5), 65.93 (C-4), 59.49, 59.43, 57.52, 21.18; HRMS *(m/z)*: $[M+Na]^+$ calcd for $C_{17}H_{24}O_6S$, 379.1191; found, 379.1189.

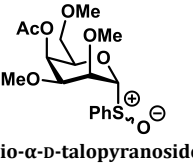

Phenyl 4-*O*-acetyl-2,3,6-tri-*O*-methyl-1-thio-α-D-talopyranoside *S*-Oxide (4). Based on a protocol by Gómez *et al.* A solution of **S16** (2 mg, 6 µmol) in DCM (0.50 mL) was cooled to –78 °C under inert atmosphere

and then *m*-CPBA (1.5 mg, 6 µmol) was added. The reaction was stirred for three hours, diluted with DCM (15 mL) and washed with 10% aq. $Na_2S_2O_3$ solution, sat. aq. $NaHCO_3$ and brine. The organic layer was dried ($MgSO_4$), filtered, concentrated *in vacuo*. The crude product **4** (2 mg) was used directly for IRMPD experiments. HRMS *(m/z)*: $[M+Na]^+$ calcd for $C_{17}H_{24}O_7S$, 395.1140; found, 395.1148.

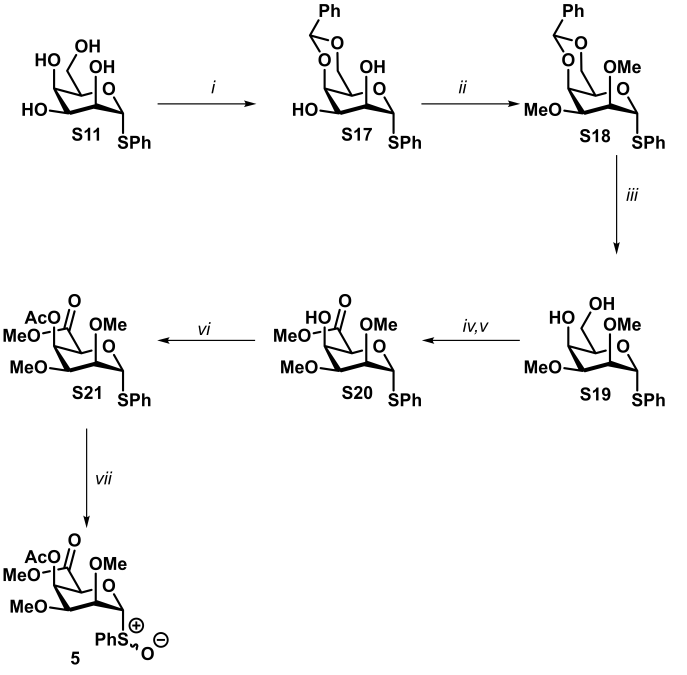

Scheme S4. *i*) α,α-dimethoxy toluene, $HBF_4.Et_2O$, DMF; **S17**, 90%; *ii*) MeI, NaH, THF/DMF; **S18**, 64%; *iii*) *p*-TsOH, MeOH; **S19**, 68%; *iv*) TEMPO, BAIB, DCM/H_2O; *v*) MeI, K_2CO_3, DMF; **S20**, 52% over two steps; *vi*) Ac_2O, pyridine; **S21**, 97%; *vii*) *m*-CPBA, DCM, **5** used as crude for IRIS.

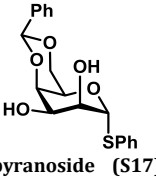

Phenyl 4,6-*O*-benzylidene-1-thio-α-D-talopyranoside (S17). To a solution of phenyl 1-thio-α-D-talopyranoside (**S11**) (1.16 g, 4.25 mmol) in anhydrous DMF (10 mL), were added while stirring under inert atmosphere at 0 °C: α,α-dimethoxy toluene (640 µL, 4.26 mmol,) and tetrafluoroboric acid diethyl etherate complex (578 µL, 4.25 mmol). After 22 h of stirring the reaction was quenched with TEA (1 mL, 7 mmol) and concentrated *in vacuo*. Silicagel flash column chromatography (0 → 40 % EtOAc in *n*-heptane) of the crude afforded **S17** as a white solid (1.37 g, 3.81 mmol, 90%). TLC: R_f 0.48, (EtOAc/*n*-heptane, 1/1, v/v); ^{1}H NMR (500 MHz, Chloroform-*d*) δ 7.49-7.45 (m, 4H), 7.39-7.37 (m, 3H), 7.34-7.26 (m, 3H), 5.78 (s, 1H, H-1), 5.53 (s, 1H, H-benzylidene), 4.34 (d, *J* = 3.4 Hz, 1H, H-4), 4.31 (dd, *J* = 12.7, 1.4 Hz, 1H, H-6a), 4.23 (s, 1H, H-5), 4.12 (dd, *J* = 12.7, 1.7 Hz, 1H, H-6b), 4.02 (m, 1H, H-2), 3.92 (dt, *J* = 3.5 Hz, 11.4 Hz, 1H, H-3), 3.53 (d, *J* = 12.2 Hz, 1H, OH-2), 2.99 (d, *J* = 11.4 Hz, 1H, OH-2); ^{13}C NMR (126 MHz, $CDCl_3$) δ 137.05, 133.78, 130.77, 129.43, 129.18, 128.44, 125.98, 101.78 (C-benzylidene), 88.94 (C-1), 76.73 (C-4), 71.62 (C-2), 69.61 (C-6), 66.20 (C-3), 63.76 (C-5); HRMS *(m/z)*: $[M+Na]^+$ calcd for $C_{19}H_{20}O_5S$, 383.0929; found, 383.0928.

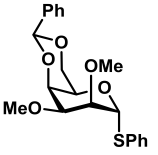

Phenyl 4,6-*O*-benzylidene-2,3-di-*O*-methyl-1-thio-α-D-talopyranoside (S18). To a mixture of **S17** (350 mg, 0.97 mmol) in THF/DMF (9.7 mL, 1/1, v/v) NaH (97 mg, 2.43 mmol, 60 %weight in mineral oil) was added. After stirring for 10 minutes, MeI (0.13 ml, 2.0 mmol) was added and the reaction was stirred overnight at rt. The mixture was quenched by addition of sat. aq. NH_4Cl and diluted with EtOAc (30 mL). The resulting emulsion was transferred to a separation funnel and washed with H_2O (30 mL) and brine (30 mL). The organic layer was dried ($MgSO_4$), filtered and concentrated *in vacuo*. Silicagel flash column chromatography (40 % EtOAc in *n*-heptane) of the crude afforded **S18** (258 mg, 64%) as a white solid. TLC: R_f 0.18, (3/7, EtOAc/heptane, v/v); ^{1}H NMR (400 MHz, Chloroform-*d*) δ 7.64 – 7.44 (m, 4H, 4 x C*H* Ar), 7.40 – 7.10 (m, 6H, 6 x C*H* Ar), 5.98 (d, *J* = 1.2 Hz, 1H, H-1), 5.52 (s, 1H, C*H* benzylidene), 4.36 (dt, *J* = 3.6, 1.0 Hz, 1H, H-4), 4.27 (dd, *J* = 12.4, 1.2 Hz, 1H, H-6A), 4.17 – 4.09 (m, 2H, H-6B, H-5), 3.82 (ddd, *J* = 3.6, 1.4, 0.7 Hz, 1H, H-2), 3.56 (t, *J* = 3.6 Hz, 1H, H-3), 3.54 (s, 3H, -OCH_3), 3.50 (s, 3H, OCH_3); ^{13}C NMR (101 MHz, Chloroform-*d*) δ 137.86, 134.59, 130.04, 129.13, 128.86, 128.09, 127.07, 126.82, 101.80, 84.97 (C-1), 77.20 (C-2), 76.20 (C-3), 72.05 (C-4), 69.81 (C-6), 63.79 (C-5), 58.76, 56.41; HRMS *(m/z)*: $[M+Na]^+$ calcd for $C_{21}H_{24}O_5S$, 411.1242; found, 411.1251.

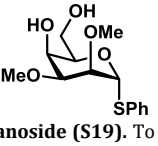

Phenyl 2,3-di-*O*-methyl-1-thio-α-D-talopyranoside (S19). To a suspension of **S18** (249 mg, 0.64 mmol) in MeOH (6.4 mL), *p*-TsOH (24 mg, 0.13 mmol) was added and stirred for 18 hours. After TLC indicated conversion, the resulting clear solution was quenched by addition of triethylamine and subsequently concentrated *in vacuo*. Silica column chromatography (EtOAc/*n*-heptane, 3/2, v/v) of the residue gave **S19** (131 mg, 68 %) as a clear oil. TLC**:** R_f 0.23, (3/2, EtOAc/heptane, v/v); ^{1}H NMR (400 MHz, Methanol-d_4) δ 7.66 – 7.51 (m, 2H, 2 x C*H* Ar), 7.49 – 7.18 (m, 3H, 3 x C*H* Ar), 5.67 (d, *J* = 1.5 Hz, 1H, H-1), 4.29 – 4.21 (m, 1H, H-5), 4.04 (dt, *J* = 3.0, 1.4 Hz, 1H, H-4), 3.88 (dt, *J* = 3.0, 1.4 Hz, 1H, H-2), 3.78 (dd, *J* = 11.4, 5.6 Hz, 1H, H-6A), 3.72 (dd, *J* = 11.4, 6.8 Hz, 1H, H-6B), 3.49 (t, *J* = 3.2 Hz, 1H, H-3), 3.48 (s, 1H, -OCH_3), 3.47 (s, 1H, -OCH_3); ^{13}C NMR (101 MHz, Methanol-d_4) δ 135.35, 133.22, 130.13, 128.79, 86.80(C-1), 81.21(C-3), 77.22(C-2), 74.34(C-5), 68.11(C-4), 62.34(C-6), 59.17, 55.96.

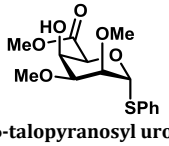

Methyl (phenyl 2,3-di-*O*-methyl-1-thio-α-D-talopyranosyl uronate) (S20). Based on a protocol by Zhang *et al.* **S19** (115 mg, 0.38 mmol) was dissolved in a mixture of H_2O and DCM (4.0 mL, 1/9, v/v). To the solution BAIB (308 mg, 0.96 mmol) and TEMPO (12 mg, 0.077 mmol) were added. The mixture was left under vigorous stirring for two hours before being quenched by 10 % aqueous $Na_2S_2O_3$ solution (2 mL). The mixture was acidified to pH 3 and extracted with EtOAc (3 x 10 mL). The organic layers were combined, dried (MgSO4), filtered and concentrated *in vacuo*. The crude residue was dissolved in DMF (3.8 mL). To the solution, K_2CO_3 (53 mg, 0.38 mmol) and MeI (48 µL, 0.76 mmol) were added. The mixture was stirred at rt before completion was observed by TLC after two hours. The mixture was diluted with EtOAc (20 mL) and washed with sat. aq. NaCl (15 mL). The organic layer was dried (MgSO4), filtered and concentrated *in vacuo*. Silica column chromatography of the residue (70% EtOAc in *n*-heptane) gave **S20** (65 mg, 52% over two steps) as a clear oil. TLC: R_f 0.42, (7/3, EtOAc/heptane, v/v); ^{1}H NMR (400 MHz, Chloroform-*d*) δ 7.58 – 7.41 (m, 2H, 2 x C*H* Ar), 7.39 – 7.21 (m, 3H, 3 x C*H* Ar), 5.82 (d, *J* = 1.7 Hz, 1H, H-1), 4.87 (d, *J* = 1.6 Hz, 1H, H-5), 4.44 (ddt, *J* = 10.8, 3.2, 1.5 Hz, 1H, H-4), 3.87 (dt, *J* = 3.0, 1.5 Hz, 1H, H-2), 3.83 (s, 3H, COOCH_3), 3.76 (dd, *J* = 10.8, 0.6 Hz, 1H, 4-O*H*), 3.52 (s, 3H, -OCH_3), 3.51 (s, 3H, -OCH_3), 3.49 – 3.46 (m, 1H, H-3); ^{13}C NMR (101 MHz, Chloroform-*d*) δ 168.85(C-6), 133.56, 131.09, 129.37, 127.85, 85.03(C-1), 79.99(C-2), 75.17(C-3), 72.96(C-5), 68.05(C-4), 58.94, 56.03, 52.57; HRMS *(m/z)*: $[M+Na]^+$ calcd for $C_{15}H_{20}O_6S$, 351.0878; found, 351.0881.

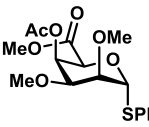

Methyl (phenyl 4-*O*-acetyl-2,3-di-*O*-methyl-1-thio-β-D-talopyranosyl uronate) (S21). To a solution of **S20** (52 mg, 0.16 mmol) in pyridine (1.0 mL), Ac_2O (0.50 mL) was added. The mixture stirred for 18 hours after which it was concentrated *in vacuo*. The residue was dissolved in EtOAc (10 mL) and washed with 10% aqueous $CuSO_4$ solution (10 mL), H_2O (10 mL) and brine (10 mL). The mixture was dried ($MgSO_4$), filtered and concentrated *in vacuo* to give the product **S21** as a pale oil (57 mg, 97%). TLC: R_f 0.29, (1/1, EtOAc/heptane, v/v); ^{1}H NMR (400 MHz, Chloroform-*d*) δ 7.58 – 7.44 (m, 2H, 2 x C*H* Ar), 7.40 – 7.20 (m, 3H, 3 x C*H* Ar), 5.87 (d, *J* = 2.0 Hz, 1H, H-1), 5.73 (t, *J* = 2.6 Hz, 1H, H-4), 5.01 (d, *J* = 2.2 Hz, 1H, H-5), 3.75 (s, 3H, COOCH_3), 3.69 (ddd, *J* = 3.4, 2.0, 0.8 Hz, 1H, H-2), 3.55 (t, *J* = 3.5 Hz, 1H, H-3), 3.50 (s, 3H, -OCH_3), 3.49 (s, 3H, -OCH_3), 2.12 (s, 3H, CH_3 Ac); ^{13}C NMR (101 MHz, Chloroform-*d*) δ 170.38, 168.03(C-6), 133.72, 130.68, 129.36, 127.63, 84.97(C-1), 78.58(C-2), 75.76(C-3), 70.23(C-5), 66.39(C-4), 59.04, 57.91, 52.59, 21.05; HRMS *(m/z)*: $[M+Na]^+$ calcd for $C_{17}H_{22}O_7S$, 393.0984; found, 393.0981.

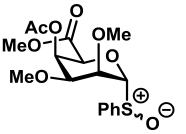

Methyl (phenyl 4-*O*-acetyl-2,3-di-*O*-methyl-1-thio-β-D-talopyranosyl uronate) *S*-Oxide (5). Based on a protocol by Gómez *et al.* A solution of **S21** (24 mg, 0.065 mmol) in DCM (1.2 mL) was cooled to –78 °C under inert atmosphere and then *m*-CPBA (18 mg, 0.071 mmol) was added. The reaction was stirred for three hours, diluted with DCM (15 mL) and washed with 10% aq. $Na_2S_2O_3$ solution, sat. aq. $NaHCO_3$ and brine. The organic layer was dried ($MgSO_4$), filtered, concentrated *in vacuo*. The crude product **5** (17 mg) was used directly for IRMPD experiments. TLC: R_f 0.31, (4/1, EtOAc/heptane, v/v); HRMS *(m/z)*: $[M+Na]^+$ calcd for $C_{17}H_{22}O_8S$, 409.0933; found, 409.0941.

References

(1) Crich, D.; Sun, S. Are Glycosyl Triflates Intermediates in the Sulfoxide Glycosylation Method? A Chemical and ^{1}H, ^{13}C, and ^{19}F NMR Spectroscopic Investigation. *J. Am. Chem. Soc.* **1997**, *119* (46), 11217–11223.

(2) Frihed, T. G.; Bols, M.; Pedersen, C. M. Mechanisms of Glycosylation Reactions Studied by Low-Temperature Nuclear Magnetic Resonance. *Chem. Rev.* **2015**, *115* (11), 4963–5013.

(3) Pittman, C. U.; McManus, S. P.; Larsen, J. W. 1,3-Dioxolan-2-Ylium and Related Heterocyclic Cations. *Chem. Rev.* **1972**, *72* (4), 357–438.

(4) Crich, D.; Dai, Z.; Gastaldi, S. On the Role of Neighboring Group Participation and Ortho Esters in β-Xylosylation: ^{13}C NMR Observation of a Bridging 2-Phenyl-1,3-Dioxalenium Ion. *J. Org. Chem.* **1999**, *64* (14), 5224–5229.

(5) Nukada, T.; Berces, A.; Zgierski, M. Z.; Whitfield, D. M. Exploring the Mechanism of Neighboring Group Assisted Glycosylation Reactions. *J. Am. Chem. Soc.* **1998**, *120* (51), 13291–13295.

(6) Santana, A. G.; Montalvillo-Jiménez, L.; Díaz-Casado, L.; Corzana, F.; Merino, P.; Cañada, F. J.; Jiménez-Osés, G.; Jiménez-Barbero, J.; Gómez, A. M.; Asensio, J. L. Dissecting the Essential Role of Anomeric β-Triflates in Glycosylation Reactions. *J. Am. Chem. Soc.* **2020**, *142* (28), 12501–12514.

(7) de Kleijne, F. F. J.; Elferink, H.; Moons, S. J.; White, P. B.; Boltje, T. J. Characterization of Mannosyl Dioxanium Ions in Solution Using Chemical Exchange Saturation Transfer NMR Spectroscopy. *Angew. Chem. Int. Ed.* **2022**, *61* (6), e202109874.

(8) Qiao, Y.; Ge, W.; Jia, L.; Hou, X.; Wang, Y.; M. Pedersen, C. Glycosylation Intermediates Studied Using Low Temperature ^{1}H- and ^{19}F-DOSY NMR: New Insight into the Activation of Trichloroacetimidates. *Chem. Commun.* **2016**, *52* (76), 11418–11421.

(9) Lu, S.-R.; Lai, Y.-H.; Chen, J.-H.; Liu, C.-Y.; Mong, K.-K. T. Dimethylformamide: An Unusual Glycosylation Modulator. *Angew. Chem. Int. Ed.* **2011**, *50* (32), 7315–7320.

(10) Seeman, J. I. Effect of Conformational Change on Reactivity in Organic Chemistry. Evaluations, Applications, and Extensions of Curtin-Hammett Winstein-Holness Kinetics. *Chem. Rev.* **1983**, *83* (2), 83–134.

(11) Seeman, J. I. The Curtin-Hammett Principle and the Winstein-Holness Equation: New Definition and Recent Extensions to Classical Concepts. *J. Chem. Educ.* **1986**, *63* (1), 42.

(12) Franconetti, A.; Ardá, A.; Asensio, J. L.; Blériot, Y.; Thibaudeau, S.; Jiménez-Barbero, J. Glycosyl Oxocarbenium Ions: Structure, Conformation, Reactivity, and Interactions. *Acc. Chem. Res.* **2021**, *54* (11), 2552–2564.

(13) Merino, P.; Delso, I.; Pereira, S.; Orta, S.; Pedrón, M.; Tejero, T. Computational Evidence of Glycosyl Cations. *Org. Biomol. Chem.* **2021**, *19* (11), 2350–2365.
(14) Hettikankanamalage, A. A.; Lassfolk, R.; Ekholm, F. S.; Leino, R.; Crich, D. Mechanisms of Stereodirecting Participation and Ester Migration from Near and Far in Glycosylation and Related Reactions. *Chem. Rev.* **2020**, *120* (15), 7104–7151.
(15) Martin, A.; Arda, A.; Désiré, J.; Martin-Mingot, A.; Probst, N.; Sinaÿ, P.; Jiménez-Barbero, J.; Thibaudeau, S.; Blériot, Y. Catching Elusive Glycosyl Cations in a Condensed Phase with HF/SbF_5 Superacid. *Nat. Chem.* **2016**, *8* (2), 186–191.
(16) Lebedel, L.; Ardá, A.; Martin, A.; Désiré, J.; Mingot, A.; Aufiero, M.; Aiguabella Font, N.; Gilmour, R.; Jiménez-Barbero, J.; Blériot, Y.; Thibaudeau, S. Structural and Computational Analysis of 2-Halogeno-Glycosyl Cations in the Presence of a Superacid: An Expansive Platform. *Angew. Chem. Int. Ed.* **2019**, *58* (39), 13758–13762.
(17) Elferink, H.; Severijnen, M. E.; Martens, J.; Mensink, R. A.; Berden, G.; Oomens, J.; Rutjes, F. P. J. T.; Rijs, A. M.; Boltje, T. J. Direct Experimental Characterization of Glycosyl Cations by Infrared Ion Spectroscopy. *J. Am. Chem. Soc.* **2018**, *140* (19), 6034–6038.
(18) Braak, F. ter; Elferink, H.; Houthuijs, K. J.; Oomens, J.; Martens, J.; Boltje, T. J. Characterization of Elusive Reaction Intermediates Using Infrared Ion Spectroscopy: Application to the Experimental Characterization of Glycosyl Cations. *Acc. Chem. Res.* **2022**, *55* (12), 1669–1679.
(19) Hansen, T.; Lebedel, L.; Remmerswaal, W. A.; van der Vorm, S.; Wander, D. P. A.; Somers, M.; Overkleeft, H. S.; Filippov, D. V.; Désiré, J.; Mingot, A.; Bleriot, Y.; van der Marel, G. A.; Thibaudeau, S.; Codée, J. D. C. Defining the S_N1 Side of Glycosylation Reactions: Stereoselectivity of Glycopyranosyl Cations. *ACS Cent. Sci.* **2019**, *5* (5), 781–788.
(20) Upadhyaya, K.; Subedi, Y. P.; Crich, D. Direct Experimental Characterization of a Bridged Bicyclic Glycosyl Dioxacarbenium Ion by ^{1}H and ^{13}C NMR Spectroscopy: Importance of Conformation on Participation by Distal Esters. *Angew. Chem. Int. Ed.* **2021**, *60* (48), 25397–25403.
(21) Crich, D. En Route to the Transformation of Glycoscience: A Chemist's Perspective on Internal and External Crossroads in Glycochemistry. *J. Am. Chem. Soc.* **2021**, *143* (1), 17–34.
(22) Mucha, E.; Marianski, M.; Xu, F.-F.; Thomas, D. A.; Meijer, G.; von Helden, G.; Seeberger, P. H.; Pagel, K. Unravelling the Structure of Glycosyl Cations via Cold-Ion Infrared Spectroscopy. *Nat. Commun.* **2018**, *9* (1), 4174.
(23) Marianski, M.; Mucha, E.; Greis, K.; Moon, S.; Pardo, A.; Kirschbaum, C.; Thomas, D. A.; Meijer, G.; von Helden, G.; Gilmore, K.; Seeberger, P. H.; Pagel, K. Remote Participation during Glycosylation Reactions of Galactose Building Blocks: Direct Evidence from Cryogenic Vibrational Spectroscopy. *Angew. Chem. Int. Ed.* **2020**, *59* (15), 6166–6171.
(24) Greis, K.; Kirschbaum, C.; Fittolani, G.; Mucha, E.; Chang, R.; von Helden, G.; Meijer, G.; Delbianco, M.; Seeberger, P. H.; Pagel, K. Neighboring Group Participation of Benzoyl Protecting Groups in C3- and C6-Fluorinated Glucose. *Eur. J. Org. Chem.* **2022**, *2022* (15), e202200255.
(25) Elferink, H.; Mensink, R. A.; Castelijns, W. W. A.; Jansen, O.; Bruekers, J. P. J.; Martens, J.; Oomens, J.; Rijs, A. M.; Boltje, T. J. The Glycosylation Mechanisms of 6,3-Uronic Acid Lactones. *Angew. Chem. Int. Ed.* **2019**, *58* (26), 8746–8751.
(26) Bérces, A.; Enright, G.; Nukada, T.; Whitfield, D. M. The Conformational Origin of the Barrier to the Formation of Neighboring Group Assistance in Glycosylation Reactions: A Dynamical Density Functional Theory Study. *J. Am. Chem. Soc.* **2001**, *123* (23), 5460–5464.
(27) Nukada, T.; Bérces, A.; Whitfield, D. M. Can the Stereochemical Outcome of Glycosylation Reactions Be Controlled by the Conformational Preferences of the Glycosyl Donor? *Carbohydr. Res.* **2002**, *337* (8), 765–774.
(28) Whitfield, D. M.; Nukada, T. DFT Studies of the Role of C-2–O-2 Bond Rotation in Neighboring-Group Glycosylation Reactions. *Carbohydr. Res.* **2007**, *342* (10), 1291–1304.
(29) Hansen, T.; Elferink, H.; van Hengst, J. M. A.; Houthuijs, K. J.; Remmerswaal, W. A.; Kromm, A.; Berden, G.; van der Vorm, S.; Rijs, A. M.; Overkleeft, H. S.; Filippov, D. V.; Rutjes, F. P. J. T.; van der Marel, G. A.; Martens, J.; Oomens, J.; Codée, J. D. C.; Boltje, T. J. Characterization of Glycosyl Dioxolenium Ions and Their Role in Glycosylation Reactions. *Nat. Commun.* **2020**, *11* (1), 2664.
(30) Liu, X.; Song, Y.; Liu, A.; Zhou, Y.; Zhu, Q.; Lin, Y.; Sun, H.; Zhu, K.; Liu, W.; Ding, N.; Xie, W.; Sun, H.; Yu, B.; Xu, P.; Li, W. More than a Leaving Group: *N*-Phenyltrifluoroacetimidate as a Remote Directing Group for Highly α-Selective 1,2-*Cis* Glycosylation. *Angew. Chem.* **2022**, *134* (21), e202201510.
(31) Panova, M. V.; Medvedev, M. G.; Orlova, A. V.; Kononov, L. O. Exhaustive Conformational Search for Sialyl Cation Reveals Possibility of Remote Participation of Acyl Groups. *ChemPhysChem* **2022**, *23* (3), e202100788.
(32) de Wildt, S. N.; Kearns, G. L.; Leeder, J. S.; van den Anker, J. N. Glucuronidation in Humans. Pharmacogenetic and Developmental Aspects. *Clin. Pharmacokinet.* **1999**, *36* (6), 439–452.
(33) Dinkelaar, J.; de Jong, A. R.; van Meer, R.; Somers, M.; Lodder, G.; Overkleeft, H. S.; Codée, J. D. C.; van der Marel, G. A. Stereodirecting Effect of the Pyranosyl C-5 Substituent in Glycosylation Reactions. *J. Org. Chem.* **2009**, *74* (14), 4982–4991.

(34) Hansen, T.; van der Vorm, S.; Tugny, C.; Remmerswaal, W. A.; van Hengst, J. M. A.; van der Marel, G. A.; Codée, J. D. C. Stereoelectronic Effects in Glycosylation Reactions. In *Reference Module in Chemistry, Molecular Sciences and Chemical Engineering*; Elsevier, 2021.
(35) Walvoort, M. T. C.; Lodder, G.; Mazurek, J.; Overkleeft, H. S.; Codée, J. D. C.; van der Marel, G. A. Equatorial Anomeric Triflates from Mannuronic Acid Esters. *J. Am. Chem. Soc.* **2009**, *131* (34), 12080–12081.
(36) Ayala, L.; Lucero, C. G.; Romero, J. A. C.; Tabacco, S. A.; Woerpel, K. A. Stereochemistry of Nucleophilic Substitution Reactions Depending upon Substituent: Evidence for Electrostatic Stabilization of Pseudoaxial Conformers of Oxocarbenium Ions by Heteroatom Substituents. *J. Am. Chem. Soc.* **2003**, *125* (50), 15521–15528.
(37) Xiao, H.; Wang, G.; Wang, P.; Li, Y. Convenient Synthesis of D-Talose from D-Galactose. *Chin. J. Chem.* **2010**, *28* (7), 1229–1232.
(38) Martens, J.; Berden, G.; Gebhardt, C. R.; Oomens, J. Infrared Ion Spectroscopy in a Modified Quadrupole Ion Trap Mass Spectrometer at the FELIX Free Electron Laser Laboratory. *Rev. Sci. Instrum.* **2016**, *87* (10), 103108.
(39) Martens, J.; Grzetic, J.; Berden, G.; Oomens, J. Structural Identification of Electron Transfer Dissociation Products in Mass Spectrometry Using Infrared Ion Spectroscopy. *Nat. Commun.* **2016**, *7* (1), 11754.
(40) Barnes, L.; Allouche, A.-R.; Chambert, S.; Schindler, B.; Compagnon, I. Ion Spectroscopy of Heterogeneous Mixtures: IRMPD and DFT Analysis of Anomers and Conformers of Monosaccharides. *Int. J. Mass Spectrom.* **2020**, *447*, 116235.
(41) Hansen, T.; Ofman, T. P.; Vlaming, J. G. C.; Gagarinov, I. A.; van Beek, J.; Goté, T. A.; Tichem, J. M.; Ruijgrok, G.; Overkleeft, H. S.; Filippov, D. V.; van der Marel, G. A.; Codée, J. D. C. Reactivity–Stereoselectivity Mapping for the Assembly of Mycobacterium Marinum Lipooligosaccharides. *Angew. Chem. Int. Ed.* **2021**, *60* (2), 937–945.
(42) Madern, J. M.; Hansen, T.; van Rijssel, E. R.; Kistemaker, H. A. V.; van der Vorm, S.; Overkleeft, H. S.; van der Marel, G. A.; Filippov, D. V.; Codée, J. D. C. Synthesis, Reactivity, and Stereoselectivity of 4-Thiofuranosides. *J. Org. Chem.* **2019**, *84* (3), 1218–1227.
(43) van der Vorm, S.; Hansen, T.; van Rijssel, E. R.; Dekkers, R.; Madern, J. M.; Overkleeft, H. S.; Filippov, D. V.; van der Marel, G. A.; Codée, J. D. C. Furanosyl Oxocarbenium Ion Conformational Energy Landscape Maps as a Tool to Study the Glycosylation Stereoselectivity of 2-Azidofuranoses, 2-Fluorofuranoses and Methyl Furanosyl Uronates. *Chem. – Eur. J.* **2019**, *25* (29), 7149–7157.
(44) Lucero, C. G.; Woerpel, K. A. Stereoselective C-Glycosylation Reactions of Pyranoses: The Conformational Preference and Reactions of the Mannosyl Cation. *J. Org. Chem.* **2006**, *71* (7), 2641–2647.
(45) The **1-TS** barrier for TalA cation **10** was found to be 33.9 kcal mol^{-1}, while for GalA cation **7** no transition state could not be located due to the barrier height (Table S1).
(46) The GluA and ManA cations **6** and **8** showed auto-fragmentation of time, and thus could not be used for isomer population analysis (See the supplementary methods for an extensive discussion on isomer population analysis).
(47) Remmerswaal, W. A.; Houthuijs, K. J.; van de Ven, R.; Elferink, H.; Hansen, T.; Berden, G.; Overkleeft, H. S.; van der Marel, G. A.; Rutjes, F. P. J. T.; Filippov, D. V.; Boltje, T. J.; Martens, J.; Oomens, J.; Codée, J. D. C. Stabilization of Glucosyl Dioxolenium Ions by "Dual Participation" of the 2,2-Dimethyl-2-(*Ortho*-Nitrophenyl)Acetyl (DMNPA) Protection Group for 1,2-*Cis*-Glucosylation. *J. Org. Chem.* **2022**, *87* (14), 9139–9147.
(48) Liu, H.; Zhou, S.-Y.; Wen, G.-E.; Liu, X.-X.; Liu, D.-Y.; Zhang, Q.-J.; Schmidt, R. R.; Sun, J.-S. The 2,2-Dimethyl-2-(*Ortho*-Nitrophenyl)Acetyl (DMNPA) Group: A Novel Protecting Group in Carbohydrate Chemistry. *Org. Lett.* **2019**, *21* (19), 8049–8052.
(49) Liu, H.; Hansen, T.; Zhou, S.-Y.; Wen, G.-E.; Liu, X.-X.; Zhang, Q.-J.; Codée, J. D. C.; Schmidt, R. R.; Sun, J.-S. Dual-Participation Protecting Group Solves the Anomeric Stereocontrol Problems in Glycosylation Reactions. *Org. Lett.* **2019**, *21* (21), 8713–8717.
(50) Rijs, A. M.; Oomens, J. IR Spectroscopic Techniques to Study Isolated Biomolecules. In *Gas-Phase IR Spectroscopy and Structure of Biological Molecules*; Rijs, A. M., Oomens, J., Eds.; Topics in Current Chemistry; Springer International Publishing: Cham, 2015; pp 1–42.
(51) van Outersterp, R.E.; Houthuijs, K.J.; Berden, G.; Engelke, U.F.; Kluijtmans, L.A.J.; Wevers, R.A.; Coene, K.L.M.; Oomens, J.; Martens, J.; Molecular Spectroscopy (HIMS, FNWI). Reference-Standard Free Metabolite Identification Using Infrared Ion Spectroscopy. *Int. J. Mass Spectrom.* **2019**, *443*, 77–85.
(52) Landrum, G.; Tosco, P.; Kelley, B.; sriniker; gedeck; NadineSchneider; Vianello, R.; Ric; Dalke, A.; Cole, B.; AlexanderSavelyev; Swain, M.; Turk, S.; N, D.; Vaucher, A.; Kawashima, E.; Wójcikowski, M.; Probst, D.; godin, guillaume; Cosgrove, D.; Pahl, A.; JP; Berenger, F.; strets123; JLVarjo; O'Boyle, N.; Fuller, P.; Jensen, J. H.; Sforna, G.; DoliathGavid. Rdkit/Rdkit: 2020_03_1 (Q1 2020) Release, 2020.
(53) Frisch, M. J.; Trucks, G. W.; Schlegel, H. B.; Scuseria, G. E.; Robb, M. A.; Cheeseman, J. R.; Scalmani, G.; Barone, V.; Petersson, G. A.; Nakatsuji, H.; Li, X.; Caricato, M.; Marenich, A. V.; Bloino, J.; Janesko, B. G.; Gomperts, R.; Mennucci, B.; Hratchian, H. P.; Ortiz, J. V.; Izmaylov, A. F.; Sonnenberg, J. L.; Williams; Ding, F.; Lipparini, F.; Egidi, F.; Goings, J.; Peng, B.; Petrone, A.; Henderson, T.; Ranasinghe, D.; Zakrzewski, V. G.; Gao, J.; Rega, N.; Zheng, G.; Liang, W.; Hada, M.; Ehara, M.; Toyota, K.; Fukuda, R.; Hasegawa, J.; Ishida,

M.; Nakajima, T.; Honda, Y.; Kitao, O.; Nakai, H.; Vreven, T.; Throssell, K.; Montgomery Jr., J. A.; Peralta, J. E.; Ogliaro, F.; Bearpark, M. J.; Heyd, J. J.; Brothers, E. N.; Kudin, K. N.; Staroverov, V. N.; Keith, T. A.; Kobayashi, R.; Normand, J.; Raghavachari, K.; Rendell, A. P.; Burant, J. C.; Iyengar, S. S.; Tomasi, J.; Cossi, M.; Millam, J. M.; Klene, M.; Adamo, C.; Cammi, R.; Ochterski, J. W.; Martin, R. L.; Morokuma, K.; Farkas, O.; Foresman, J. B.; Fox, D. J. Gaussian 16 Rev. C.01, 2016.

(54) Pedregosa, F.; Varoquaux, G.; Gramfort, A.; Michel, V.; Thirion, B.; Grisel, O.; Blondel, M.; Prettenhofer, P.; Weiss, R.; Dubourg, V.; Vanderplas, J.; Passos, A.; Cournapeau, D.; Brucher, M.; Perrot, M.; Duchesnay, É. Scikit-Learn: Machine Learning in Python. *J. Mach. Learn. Res.* **2011**, *12* (85), 2825–2830.

(55) Spartan'14, Wavefunction, Inc., Irvine, CA.

(56) Halgren, T. A. Merck Molecular Force Field. I. Basis, Form, Scope, Parameterization, and Performance of MMFF94. *J. Comput. Chem.* **1996**, *17* (5–6), 490–519.

(57) Frisch, M. J.; Trucks, G. W.; Cheeseman, J. R.; Scalmani, G.; Caricato, M.; Hratchian, H. P.; Li, X.; Barone, V.; Bloino, J.; Zheng, G.; Vreven, T.; Montgomery, J. A.; Petersson, G. A.; Scuseria, G. E.; Schlegel, H. B.; Nakatsuji, H.; Izmaylov, A. F.; Martin, R. L.; Sonnenberg, J. L.; Peralta, J. E.; Heyd, J. J.; Brothers, E.; Ogliaro, F.; Bearpark, M.; Robb, M. A.; Mennucci, B.; Kudin, K. N.; Staroverov, V. N.; Kobayashi, R.; Normand, J.; Rendell, A.; Gomperts, R.; Zakrzewski, V. G.; Hada, M.; Ehara, M.; Toyota, K.; Fukuda, R.; Hasegawa, J.; Ishida, M.; Nakajima, T.; Honda, Y.; Kitao, O.; Nakai, H. Gaussian 09 Rev. D.01, 2009.

(58) Hansen, T.; Lebedel, L.; Remmerswaal, W. A.; van der Vorm, S.; Wander, D. P. A.; Somers, M.; Overkleeft, H. S.; Filippov, D. V.; Désiré, J.; Mingot, A.; Bleriot, Y.; van der Marel, G. A.; Thibaudeau, S.; Codée, J. D. C. Defining the SN1 Side of Glycosylation Reactions: Stereoselectivity of Glycopyranosyl Cations. *ACS Cent. Sci.* **2019**, *5* (5), 781–788.

(59) Ribeiro, R. F.; Marenich, A. V.; Cramer, C. J.; Truhlar, D. G. Use of Solution-Phase Vibrational Frequencies in Continuum Models for the Free Energy of Solvation. *J. Phys. Chem. B* **2011**, *115* (49), 14556–14562.

(60) OriginPro, 9.0.0. OriginLab Corporation, Northampton, MA, USA.

(61) Prell, J. S.; Chang, T. M.; Biles, J. A.; Berden, G.; Oomens, J.; Williams, E. R. Isomer Population Analysis of Gaseous Ions From Infrared Multiple Photon Dissociation Kinetics. *J. Phys. Chem. A* **2011**, *115* (13), 2745–2751.

(62) van Geenen, F. A. M. G.; Kranenburg, R. F.; van Asten, A. C.; Martens, J.; Oomens, J.; Berden, G. Isomer-Specific Two-Color Double-Resonance IR2MS3 Ion Spectroscopy Using a Single Laser: Application in the Identification of Novel Psychoactive Substances. *Anal. Chem.* **2021**, *93* (4), 2687–2693.

(63) Blom, P.; Ruttens, B.; Van Hoof, S.; Hubrecht, I.; Van der Eycken, J.; Sas, B.; Van hemel, J.; Vandenkerckhove, J. A Convergent Ring-Closing Metathesis Approach to Carbohydrate-Based Macrolides with Potential Antibiotic Activity. *J. Org. Chem.* **2005**, *70* (24), 10109–10112.

(64) Chervenak, M. C.; Toone, E. J. Analysis of the Binding Specificities of Oligomannoside-Binding Proteins Using Methylated Monosaccharides. *Bioorg. Med. Chem.* **1996**, *4* (11), 1963–1977.

(65) Zhang, Q.; Howell, P. L.; Overkleeft, H. S.; Filippov, D. V.; van der Marel, G. A.; Codée, J. D. C. Chemical Synthesis of Guanosine Diphosphate Mannuronic Acid (GDP-ManA) and Its C-4-*O*-Methyl and C-4-Deoxy Congeners. *Carbohydr. Res.* **2017**, *450*, 12–18.

(66) Tam, P. H.; Lowary, T. L. Epimeric and Amino Disaccharide Analogs as Probes of an α-(1→6)-Mannosyltransferase Involved in Mycobacterial Lipoarabinomannan Biosynthesis. *Org. Biomol. Chem.* **2009**, *8* (1), 181–192.